Fundamental Research 5 (2025) 767–781

Contents lists available at ScienceDirect

Fundamental Research

journal homepage: http://www.keaipublishing.com/en/journals/fundamental-research/

Review

Recent advances in endohedral metallofullerenes

Wenting Cai [a], Mengmeng Zhang [b], Luis Echegoyen [c,d,*], Xing Lu [e,*]

[a] School of Chemistry, Xi'an Jiaotong University, Xi'an 710049, China
[b] Alan G. MacDiarmid NanoTech Institute, The University of Texas at Dallas, Richardson, TX 75080, United States
[c] Department of Chemistry, The University of Texas at El Paso, El Paso, TX 79968, United States
[d] Institute of Chemical Research of Catalonia (ICIQ), The Barcelona Institute of Science and Technology, Tarragona 43007, Spain
[e] State Key Laboratory of Materials Processing and Die & Mould Technology, School of Materials Science and Engineering, Huazhong University of Science and Technology, Wuhan 430074, China

ARTICLE INFO

Article history:
Received 14 June 2023
Received in revised form 18 October 2023
Accepted 5 December 2023
Available online 29 December 2023

Keywords:
Fullerenes
Metallofullerenes
Crystallography
Single-molecule magnet
Metal-metal bonding

ABSTRACT

Fullerenes are a collection of closed polycyclic polymers consisting exclusively of carbon atoms. Recent remarkable advancements in the fabrication of metal-fullerene nanocatalysts and polymeric fullerene layers have significantly expanded the potential applications of fullerenes in various domains, including electrocatalysis, transistors, energy storage devices, and superconductors. Notably, the interior of fullerenes provides an optimal environment for stabilizing a diverse range of metal ions or clusters through electron transfer, resulting in the formation of a novel class of hybrid molecules referred to as endohedral metallofullerenes (EMFs). The utilization of advanced synthetic methodologies and the progress achieved in separation techniques have played a pivotal role in expanding the diversity of the encapsulated metal constituents, consequently leading to distinctive structural, electronic, and physicochemical properties of novel EMFs that surpass conventional ones. Intriguing phenomena, including regioselective dimerization between EMFs, direct metal-metal bonding, and non-classical cage preferences, have been unveiled, offering valuable insights into the coordination interactions between metallic species and carbon. Of particular importance, the recent achievements in the comprehensive characterization of EMFs based on transition metals and actinide metals have generated a particular interest in the exploration of new metal clusters possessing long-desired bonding features within the realm of coordination chemistry. These clusters exhibit a remarkable affinity for coordinating with non-metal atoms such as carbon, nitrogen, oxygen, and sulfur, thus making them highly intriguing subjects of systematic investigations focusing on their electronic structures and physicochemical properties, ultimately leading to a deeper comprehension of their unparalleled bonding characteristics. Moreover, the versatility conferred by the encapsulated species endows EMFs with multifunctional properties, thereby unveiling potential applications in various fields including biomedicine, single-molecule magnets, and electronic devices.

1. Introduction

In 1985, a seminal breakthrough was achieved by Kroto, Smalley, Curl and coworkers during a series of experiments aimed at elucidating the formation of long-chain carbon molecules in celestial environments. Through laser vaporization of a graphite disk, they successfully detected the presence of C_{60} named as fullerene in short, thus unveiling its remarkable spherical structure and the presence of pi-electrons on the surface [1]. This unexpected finding, recognized by the Nobel Prize in Chemistry in 1996, served as a catalyst for the subsequent exploration and advancement of nanocarbon chemistry. As the sole molecular allotrope of elemental carbon, fullerenes exhibit diverse chemical properties, well-defined molecular structures and outstanding physicochemical properties. Over the past years, numerous valuable materials derived from fullerenes have been developed, finding applications in a wide range of disciplines including biology, medicine, electronics, and photovoltaics.

Remarkably, the interior of fullerenes exhibits a capability to accommodate metal ions or clusters, leading to the formation of hybrid materials characterized by strong metal-carbon interactions and unique electronic structures, called endohedral metallofullerenes (EMFs) [2–5]. In 1985, Smalley reported the first solvent extractable endohedral metallofullerene, La@C_{82}, unveiling a fascinating phenomenon involving a three-electron transfer from the entrapped La ion to the C_{82} fullerene cage [6–8]. This intramolecular charge transfer confers EMFs with the ability to stabilize a wide range of isolated metal ions and reactive metal clusters, thus offering an avenue for fundamental investigations into unprecedented bonding features and potential applications that were pre-

* Corresponding authors.
E-mail addresses: echegoyen@utep.edu (L. Echegoyen), lux@hust.edu.cn (X. Lu).

https://doi.org/10.1016/j.fmre.2023.12.004

viously inaccessible with empty fullerenes. Over the last decade, considerable efforts have been dedicated to the encapsulation of various metals within fullerenes, primarily employing the highly effective arc discharge method. While Group-3 (Sc, Y) and lanthanide metals have been extensively investigated and represent the most versatile and intriguing branches of EMFs, recent breakthroughs in metallofullerene research have unveiled the discovery of EMFs containing transition metals and actinides [9]. The considerably strong host-guest interactions arising from a formal four or five-electron transfer from the metal to the cage not only stabilize pentagon adjacencies on the fullerene cage but also give rise to novel configurations of metal clusters within the cage. These developments provide new insights into the potential applications in such areas as magnetic resonance imaging contrast agents, single-molecule magnets, and electron-spin quantum computing. In this comprehensive review, our main focus is to provide an overview of recent advancements in the field of EMFs, encompassing improved synthesis and purification methodologies, new members of the EMF family, comprehensive understanding of the formation mechanisms, and the potential applications of EMFs in diverse fields such as nanomedicine, single-molecule magnets, and electronic devices.

2. Novel exploration in the studies of fullerenes

2.1. Monolayer fullerene network

Carbon, as one of the most versatile elements in the periodic table, exhibits a remarkable ability to form bonds with itself and almost all other elements through sp, sp^2, and sp^3 hybridizations. Diamond and graphite, the two well-known carbon allotropes, are characterized by extended networks of sp^3-hybridized and sp^2-hybridized atoms, respectively [2]. By combining different hybridizations and geometries of carbon, it is possible to create numerous synthetic allotropes. Graphene, as a prominent synthetic carbon allotrope, has garnered significant attention due to its two-dimensional (2D) structure and exceptional carrier transport properties arising from its conjugated carbon network with unique π-electron system [10–13]. In efforts to complement the zero-bandgap nature of graphene, extensive research has been focused on the identification of other 2D carbon materials [14–17]. However, the preparation of large-sized single-crystal 2D carbon materials with moderate bandgaps remains challenging [18]. In contrast to structural units comprising single atoms, 2D structures constructed from nanoclusters are anticipated to possess improved topologies and distinctive properties. In this context, fullerene C_{60}, a representative carbon cluster, is particularly intriguing for the formation of atomic-scale 2D carbon materials through polymerization. Such polymeric fullerene layers are expected to exhibit regularly undulating topologies with a repeating arrangement of carbon clusters in a 2D plane, offering interesting electronic and magnetic properties [19–21]. Recently, 2D carbon materials composed of covalently bonded C_{60} molecules in a periodic nanocluster network structure have been successfully synthesized using various methods. Zheng et al. achieved the fabrication of monolayer polymeric C_{60} through an organic cation slicing approach, obtaining both monolayer and few-layer polymeric C_{60} with distinct quasi-hexagonal and quasi-tetragonal bulk single crystals (Fig. 1) [22]. The monolayer polymeric C_{60} features covalently bonded cluster cages of C_{60} in a plane, exhibiting high crystallinity, good thermodynamic stability, and a moderate bandgap of approximately 1.6 eV. Furthermore, the asymmetric lattice structure imparts notable in-plane anisotropic properties to the monolayer polymeric C_{60}. However, challenges remain in addressing solvent residue resulting from solution exfoliation, despite efforts to neutralize the ionic sheets using hydrogen peroxide. To overcome this, Roy et al. presented a straightforward synthesis of another 2D polymer of C_{60} that enables the production of large flakes via mechanical exfoliation, thereby yielding high-quality molecularly thin flakes with clean interfaces [23]. The synthesis of polymeric fullerene layers offers a promising avenue for the systematic design of materials, enabling the construction of 2D heterostructures characterized by distinctive topological structures and captivating properties. Consequently, these advances open up possibilities for potential applications in diverse areas, including transistors, energy storage devices, superconductors, confined light manipulation, and quantum-materials-based devices [13,16,24,25].

2.2. Metal-fullerene nanocatalysts

The unique electronic properties of fullerenes, such as high electron affinity, have also brought new possibilities for the exploration of novel applications. For instance, Forrest et al. demonstrated centimetre-scale diffusion of electrons within a photoactive, fullerene-based organic heterostructure, revealing exceptionally long diffusion lengths surpassing 3.5 cm [26]. This remarkable long-range electron diffusion observed in fullerene devices highlights their advantageous potential in optoelectronic applications when compared to conventional organic semiconductors, which typically exhibit limited charge-diffusion lengths of less than a micrometre. In addition, non-ferromagnetic materials such as diamagnetic Cu and paramagnetic Mn can undergo modifications in magnetization through charge transfer at molecular interfaces between metal films and fullerenes [27]. The C_{60}/transition metal complexes exhibit strong interfacial $3d_z$-p coupling and interface reconstruction, enabling them to surpass the Stoner criterion and display ferromagnetic behavior at room temperature. The fullerenes can also modulate the electronic density of Cu species by accepting electrons from Cu, while providing electron feedback to electron-deficient copper, thus conferring beneficial redox properties during catalysis. In a recent study, Xie et al. utilized C_{60} as an electronic buffer to regulate the electronic density of active Cu species and overcome limitations associated with conventional Cu catalysts, which can selectively hydrogenate dimethyl oxalate (DMO) to Ethylene glycol (EG) but exhibit limited activity and stability at low pressure (Fig. 1) [28]. They achieved an impressive EG yield of up to 98% ± 1% in the hydrogenation of DMO using a C_{60}_Cu/SiO_2 catalyst under ambient pressure and temperatures of 180 °C to 190 °C. Notably, the majority of C_{60} was found to be loaded on the Cu surface without intercalating into Cu lattice sites, thereby preserving the surface structure of Cu nanoparticles. The C_{60} species (C_{60} and C_{60}^-) served as single-electron acceptors from Cu^0 or single-electron donors to Cu^{2+}, thereby stabilizing Cu^+ and inhibiting its transformation to Cu^0 or Cu^{2+}. Apart from DMO hydrogenation, the use of C_{60} as an electron buffer in Cu/SiO_2 catalysts to enhance hydrogen absorption also holds potential for other copper-catalyzed hydrogenation reactions. Specifically, the C_{60}_Cu/SiO_2 catalyst was found to exhibit advantages in the electrocatalytic reduction of CO_2 to CO, enabling the CO_2-to-EG process to be carried out under ambient conditions. The investigation of C_{60}_Cu/SiO_2 catalyst represents a significant advancement in the design of high-performance electrocatalysts. This exploration has provided fresh insights into the development of novel approaches to overcome the limitations encountered by conventional catalysts. Subsequent studies have further contributed to this field, exemplified by a Pt/C_{60} single-atom catalyst [29] and the C_{60}-based pentagonal defect-rich nanocarbon electrocatalyst [30]. Likewise, the very recently reported N-doped defect-rich carbon nano-onions (CNOs), which were synthesized using C_{60} as sacrificial seeds, have also demonstrated to be high-performance carbon-based electrocatalysts [31]. These studies offer promising avenues for enhancing catalytic performance through innovative strategies and pave the way for potential breakthroughs in the field of electrocatalysis.

3. Improvement in the synthesis and purification of EMFs

In 1990, Krätschmer and Huffman successfully accomplished the large-scale synthesis of the abundant C_{60} and C_{70} fullerenes through the resistive heating of graphite in a helium atmosphere within a furnace [32]. This landmark achievement paved the way for further advancements in fullerene synthesis. Subsequently, Smalley introduced a modi-

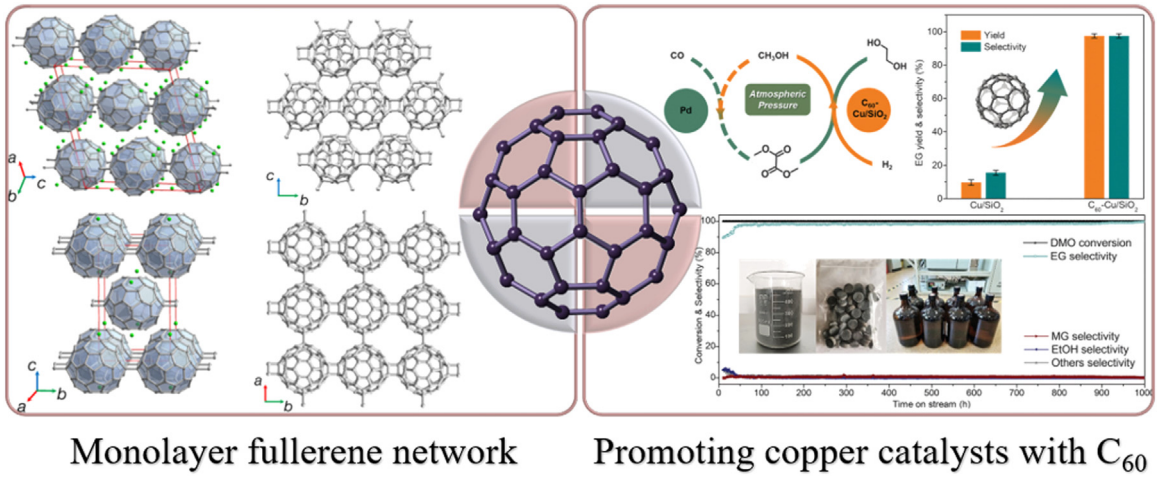

Fig. 1. Novel exploration in the studies of fullerenes. Left: crystal structures of quasi-hexagonal C_{60} and quasi-tetragonal C_{60} [22]. Right: catalytic performance of Cu/SiO_2 and C_{60}_Cu/SiO_2 at 1 bar, H_2/DMO = 200 (v/v, volume ratio), temperature 190 °C [28]. Copyright 2022, Springer Nature. Copyright 2022, The American Association for the Advancement of Science.

fied version of the Krätschmer-Huffman fullerene reactor, employing an electric arc discharge between graphite electrodes to induce a plasma. This technique has since become the predominant approach employed for fullerene production [33]. The arc discharge generates extremely high temperatures in the center, while a decreasing temperature gradient allows for the formation and stabilization of fullerenes at cooler regions.

In comparison to the conventional arc-discharge method, the combustion method has shown notable efficiency in facilitating the industrial-scale synthesis of fullerenes. The application of low-pressure combustion, coupled with an appropriate C/O ratio, was initially reported in 1991 as a viable approach for fullerene synthesis [34]. However, the underlying reaction mechanism governing the formation of fullerenes and the growth of carbon particles during combustion remains poorly understood. Moreover, the composition of fullerene species within the carbon soot generated through combustion is highly complex [35].

Even though most fullerenes and their hydrogenated derivatives obtained from combustion soot strictly adhered to the Isolated Pentagon Rule (IPR), which stipulates that a stable fullerene should have its 12 pentagons separated from each other, recent reports showed that non-IPR fullerenes are produced through combustion, such as a C_{64} molecule with three directly-fused pentagons and an isomeric form of C_{60} with double-fused pentagons [36,37]. Additionally, the smaller C_{50} fullerene, featuring 10 pairs of double-fused pentagons, has also been identified in combustion soot [38]. In 2019, Xie et al. presented an interesting non-IPR hydrofullerene, $C_{66}H_4$, which was obtained in a low-pressure diffusion flame of benzene, acetylene, and oxygen [39]. The unique structure of $C_{66}H_4$ was unambiguously determined through single-crystal X-ray diffraction, revealing a nonclassical geometry characterized by two heptagons and two pairs of fused pentagons with C_{2v} symmetry. The shared vertices of the fused pentagons are bonded to four hydrogen atoms, inducing a conversion of the sp^2 hybridization of the carbon atoms at the hydrogen-linking sites to sp^3 hybridization. This hydrogenation, coupled with the adjacent heptagons, effectively alleviates the sp^2-bond strains present at the abutting-pentagon positions of the diheptagonal fused pentagon in C_{66}. Computations indicate that the *in-situ* hydrogenation process plays a crucial role in stabilizing the diheptagonal $C_{66}H_4$, which significantly differs from the previously stabilized four isomers of C_{66} obtained through arc-discharge experiments [40–42]. This diheptagonal C_{66} structure represents the first instance of a fullerene cage with two heptagons captured during an *in-situ* carbon-clustering growth process occurring under the combustion conditions.

Similar to the synthesis of empty fullerenes, endohedral metallofullerenes (EMFs) are typically produced using an arc-discharge methodology. In this process, a target rod consisting of a mixture of metal oxides and graphite powder is subjected to arcing under direct current conditions. This results in the formation of a carbon-rich plasma under an inert gas atmosphere of helium or argon, along with the appropriate reactive gas, such as hydrogen, nitrogen, oxygen, or ammonia [5]. However, the arc-discharge method for synthesizing EMFs is known to be challenging as it lacks selectivity, leading to the production of complex mixtures containing various empty fullerenes, EMFs, nanotubes, and amorphous carbon. Although efficient high-performance liquid chromatography (HPLC) columns for separating EMFs are available, the purification of EMFs through chromatographic techniques presents significant challenges. This is primarily due to the diverse range of species present in fullerene extracts and the similarity in size and shape among carbon cages. Additionally, the content of EMFs in the extracts is typically limited, further complicating the purification process, even with the utilization of multi-step or recycling HPLC approaches [43].

In order to overcome the challenges associated with chromatographic purification, alternative non-chromatographic separation techniques have been developed, particularly focusing on endohedral metallofullerenes (EMFs). In 2005, Echegoyen and colleagues achieved a significant milestone by successfully separating $Sc_3N@I_h$-C_{80} and $Sc_3N@D_{5h}$-C_{80} isomers through selective chemical oxidation, marking a leading advancement in this field [44]. Subsequently, various versatile strategies have emerged, capitalizing on the distinctive chemical reactivity of EMFs compared to empty fullerenes, effective for the separation and purification of EMFs. These strategies include the utilization of Diels Alder (DA) reactions [45,46], the SAFA (stir and filter approach) methodology [47–49], the employment of Lewis acids [50–52], and in situ reduction induced by reflux in N,N-dimethylformamide (DMF) [53].

An alternative and promising approach for purifying EMFs involves their recognition by supramolecular receptors, leveraging their facile conformational and electronic tunability. Pioneering work by Anderson and colleagues in 2010 demonstrated the host-guest complexation of EMFs using a metalloporphyrin-based receptor [54]. Specifically, molecular receptors incorporating three porphyrins exhibited remarkably high affinities for $La@C_{82}$. The strong binding observed can be attributed to the electronic polarization of $La@C_{82}$ as well as the size and shape complementarity between $La@C_{82}$ and the molecular receptor.

Supramolecular purification strategies utilizing nanocapsules has gained momentum as highly selective platforms for isolating EMFs from carbon soot based on cage size and metallocluster composition. In 2017,

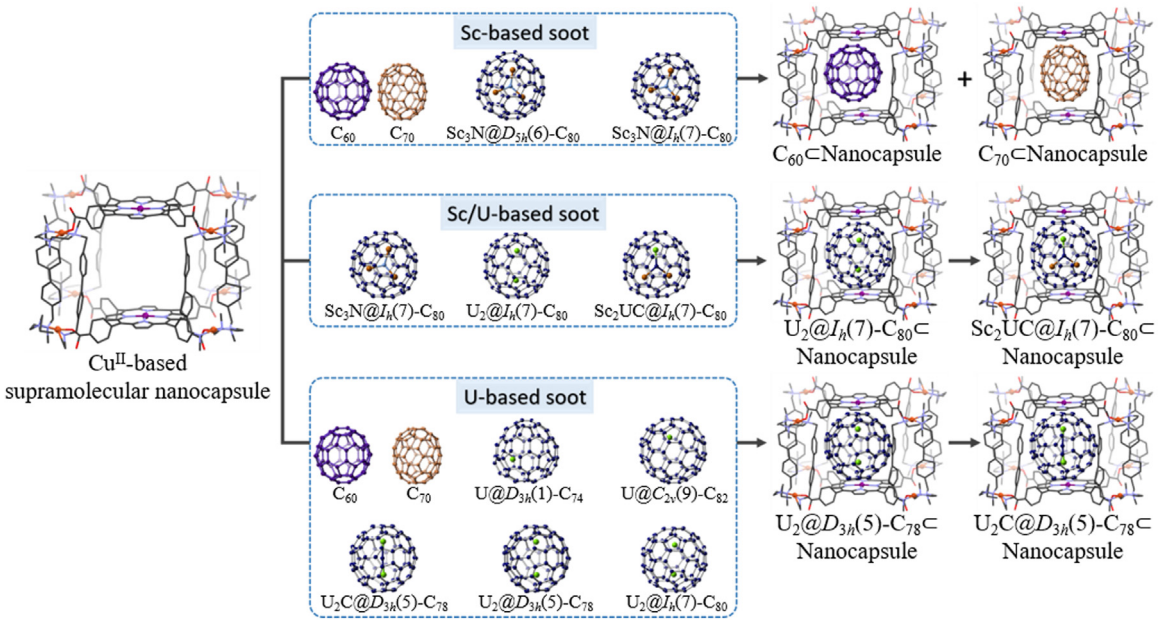

Fig. 2. Straightforward purification methodology to the desired EMFs. Selective isolation of different types of EMFs from raw soot using a Cu^{II}-based supramolecular nanocapsule.

Ribas and coworkers reported the use of a supramolecular nanocapsule capable of purifying various EMF extracts with remarkable selectivity through reversible host-guest reactions [55]. The nanocapsule, assembled from two tetracarboxylate Zn^{II}-porphyrin segments and four Cu^{II}-based macrocyclic clips, facilitated efficient entrapment of smaller cages (C_{60} and C_{70}), while larger Sc_3N-based EMFs ($Sc_3N@I_h(7)$-C_{80} and $Sc_3N@D_{5h}(6)$-C_{80}) remained in solution (Fig. 2). Leveraging these size-dependent differential affinities, $Sc_3N@C_{80}$ was successfully isolated from a mixture containing empty fullerenes and Sc_3N-containing EMFs with exceptionally high purity. In 2018, this nanocapsule demonstrated selective separation of a series of U-based actinide EMFs from U/Sc-based soot [56]. The nanocapsule crystals, when immersed in a toluene solution of soot extract containing empty fullerenes, Sc- and U-based EMFs, exhibited preferential capture of $U_2@I_h(7)$-C_{80}. Following the complete extraction of $U_2@I_h(7)$-C_{80} from the crude mixture, subsequent selective encapsulation of the unprecedented $Sc_2CU@I_h(7)$-C_{80} with the same number of transferred charges as observed for $U_2@I_h(7)$-C_{80} was achieved using the same protocol (Fig. 2). These findings confirmed that the nanocapsule selectively responded to the nature of the distinct internal clusters trapped within the fullerene cages. Calculations indicated that the highly directional electron-density distribution of U-based fullerenes, induced by the host-guest interaction, likely underlies the observed discrimination ability.

In 2019, the nanocapsule was employed for purifying a mixture of empty fullerenes and U-based EMFs of different cage sizes, including $U@C_{74}$, $U@C_{84}$, $U_2@C_{78}$, $U_2@C_{80}$, and $U_2C@C_{78}$ [57]. The remarkable selective binding enabled the isolation of pure $U_2@C_{78}$ in a single step. Subsequently, by exposing the remaining mixture to additional nanocapsule crystals, pure $U_2C@C_{78}$ was selectively complexed (Fig. 2). An in-depth examination of the host-guest selectivity revealed a smaller energy destabilization of the system upon porphyrin compression, attributable to the cylindrical shape of the $D_{3h}(5)$-C_{78} cage. Consequently, the nanocapsule exhibited a lower energy penalty during encapsulation of the elongated $D_{3h}(5)$-C_{78} compared to the spherical $I_h(7)$-C_{80}. Importantly, all encapsulated fullerenes could be easily released via a solvent-washing procedure, showcasing the potential of this straightforward methodology for practical and nonchromatographic EMF purification. The development of such streamlined purification protocols is crucial to ensure the availability of large quantities of pure EMFs for further studies, particularly for EMF derivatization and potential applications.

4. Novel phenomena in recently reported EMFs

Macroscopic synthesis of EMFs was successfully accomplished by the Smalley group in 1985, and the first solvent extraction of La-EMFs was described in 1991. The distinct electronic structure of $La@C_{2n}$ demonstrated a three-electron transfer from the entrapped La atom to the fullerene cage [7,8]. Such intramolecular charge transfer endows EMFs with unique properties that are not attainable by empty fullerenes. A significant breakthrough in fullerene research occurred in 1999 with the discovery of $Sc_3N@C_{80}$, marking the first member of Sc-EMFs [58]. This discovery was particularly significant due to the notably high yield of $Sc_3N@C_{80}$ compared to the other reported EMFs, propelling EMF research forward [43]. Comprehensive experimental and theoretical investigations concluded the six-electron transfer occurs from the entrapped Sc_3N cluster to the C_{80} cage, resulting in the mutual stabilization of the internal nitride cluster and the external cage with a specific isomeric structure. Thereafter, significant strides were made in the discovery of several other types of La-based or Sc-based metal clusters stabilized by fullerene cages, such as di-metal species, nitride cluster, carbide cluster, oxide cluster, sulfide cluster, cyanide cluster and so on. Systematic investigations on carbide cluster metallofullerenes unveiled a notable "size effect" between the encapsulated metal cluster and the fullerene cage. By leveraging the geometric effect, a series of large fullerenes (C_{90}–C_{104}) were successfully stabilized through the encapsulation of a large La_2C_2 cluster, while the relatively smaller cages (C_{72}–C_{88}) tend to accommodate the smaller Sc_2C_2 cluster [59–61].

4.1. Regioselective dimerization of pristine EMFs

Despite the significance of La-EMFs and Sc-EMFs as highly diverse and interesting branches of endohedral fullerenes, extensive efforts have been dedicated to encapsulating metals of various types inside fullerenes using the relatively effective arc discharge method. The incorporation of different metal species within fullerenes introduces novel structures and unexpected phenomena to the field of EMFs, thereby offering valuable insights into modern chemistry. Notably, intriguing regioselective

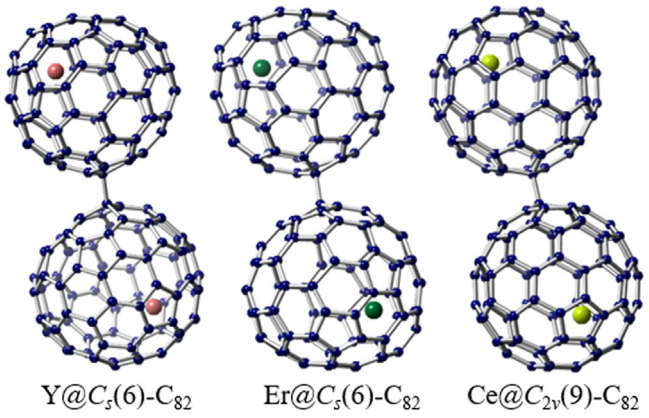

Fig. 3. Regioselective dimerization between EMFs. Drawings of the dimers of pristine metallofullerenes: Y@C_s(6)-C_{82}, Er@C_s(6)-C_{82}, and Ce@C_{2v}(9)-C_{82}. Only the major metal sites and major cage orientation are shown. The Y atoms are highlighted in red, the Er atoms are highlighted in green, and the Ce atoms are highlighted in yellow green.

dimerization phenomena have been observed in the crystalline states of Y@C_s(6)-C_{82}, Er@C_s(6)-C_{82}, and Ce@C_{2v}(9)-C_{82} when co-crystallized with Ni^{II}(OEP) (octaethylporphyrin dianion) (Fig. 3). These dimers involve the connection of two fullerene cages through a C–C single bond [62–64]. However, in the case of La-EMFs and Sc-EMFs, dimerization does not occur during the crystallization process. The formation of a similar dimer was only achieved through the synthesis of a bis-adduct of La@C_{2v}(9)-C_{82} [65]. Density functional theory calculations suggest that the regioselective dimer formation can be attributed to the localization of high spin density and pyramidalization resulting from the encapsulation of Y, Er, and Ce within the fullerene cage. Moreover, the predominant metal centers in the dimers are in close proximity to the porphyrin molecules, while the sites of dimerization are situated far from the respective inner metal atoms. This indicates that the location of the metal atom may exert a crucial influence on the spin distribution.

4.2. Direct metal-metal bonding in pristine EMFs

In addition to mono-EMFs, the emergence of di-EMFs featuring diverse metal species offers significant opportunities for investigating metal-metal bonding and gaining new insights into fullerene chemistry. Experimental confirmation of the metal-metal bond was initially reported in the triazinyl radical monoadduct and benzyl radical monoadduct of La_2@I_h(7)-C_{80} [66,67]. The addition of triazinyl radicals or benzyl radicals to the closed-shell La_2@I_h(7)-C_{80} resulted in the formation of open-shell monoadducts, namely La_2@I_h(7)-C_{80}($C_3N_3Ph_2$) or La_2@I_h(7)-C_{80}(CH_2Ph), featuring a single-electron localized in the La-La bond within the cage (Fig. 4). It has been demonstrated that the unpaired electron is transferred to the molecular orbital of the internal La_2 unit upon the addition of triazinyl radical or benzyl radical to La_2@I_h(7)-C_{80}, leading to the formation of a single-electron La-La bond. In contrast, other encapsulated lanthanide dimers within I_h(7)-C_{80}, such as M_2@I_h(7)-C_{80} (M = Y, Gd, Dy, Tb, etc.), exhibited a single-electron occupied M-M bond due to a different energy level alignment between the molecular orbital of M-M bonding and the fullerene cage (Fig. 4) [68,69]. In these cases, only one unpaired electron occupies the M-M bonding molecular orbital, while the other electron is delocalized over the fullerene cage, resulting in a formal oxidation state of +2.5 for the metal ion. However, these molecules are typically unstable radicals that are stabilized in the form of their benzyl radical monoadducts or azafullerenes by substituting a carbon atom in the cage by a nitrogen atom.

Conversely, recent experimental evidence from a series of Lu_2@$C_{76–88}$ isomers has provided the first conclusive confirmation

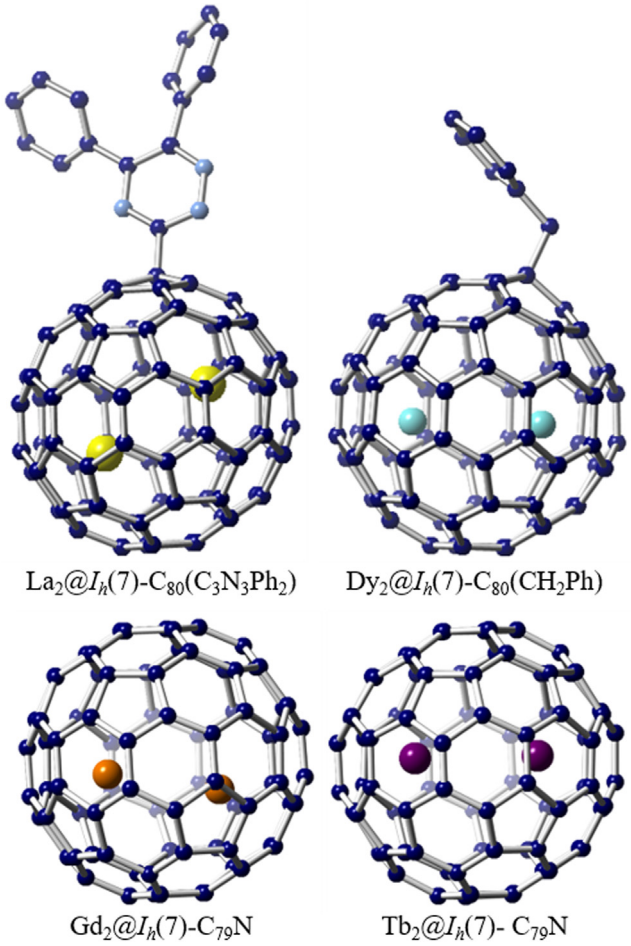

Fig. 4. Metal-metal bonding in functionalized EMFs. Drawings show the single crystal X-ray examples of benzyl radical monoadducts or azafullerenes: La_2@I_h(7)-C_{80}($C_3N_3Ph_2$), Dy_2@I_h(7)-C_{80}(CH_2Ph), Gd_2@I_h(7)-C_{79}N and Tb_2@I_h(7)-C_{79}N. The La atoms are highlighted in yellow, the Dy atoms are highlighted in light blue, the Gd atoms are highlighted in orange, and the Tb atoms are highlighted in purple.

of the metal-metal bond in pristine (unfunctionalized) EMFs (Fig. 5) [70,71]. Crystallographic analysis revealed that the distances between the two Lu atoms in these isomers fall within the range of a Lu-Lu single bond length, thereby unequivocally confirming direct Lu-Lu bonding between the repulsive Lu^{2+} ions. Theoretical calculations further support the thermodynamic favorability of Lu_2@$C_{82–86}$ isomers due to the formation of the two-electron occupied Lu-Lu bond. The hybrid composition of Lu-Lu bonds demonstrates that the Lu 6s orbital contributes significantly to the metal bonding molecular orbitals. Consequently, in these di-lutetium EMFs, each Lu atom contributes one 6s electron and one 5d electron to the fullerene cage, leading to the establishment of a formal divalent state for each Lu ion. Similarly, direct metal-metal bonds have also been identified for Y$_2$@C_{3v}(8)-C_{82} and a series of Er_2@$C_{82–86}$ isomers (Fig. 5) [72,73]. It is noteworthy that for Er_2@C_s(6)-C_{82}, Er_2@C_{3v}(8)-C_{82}, and Er_2@C_{2v}(9)-C_{86}, the two Er ions establish a two-electron occupied Er-Er bond, while Y_2@C_{3v}(8)-C_{82} and Er_2@C_1(12)-C_{84} exhibit a single-electron occupied M-M (M = Y, Er) bond, highlighting distinct bonding characteristics of the identical metallic units within different fullerene cages.

4.3. Specific non-IPR cage preferences

The incorporation of different combinations of metals and/or nonmetal atoms within metallofullerenes also results in a diverse composi-

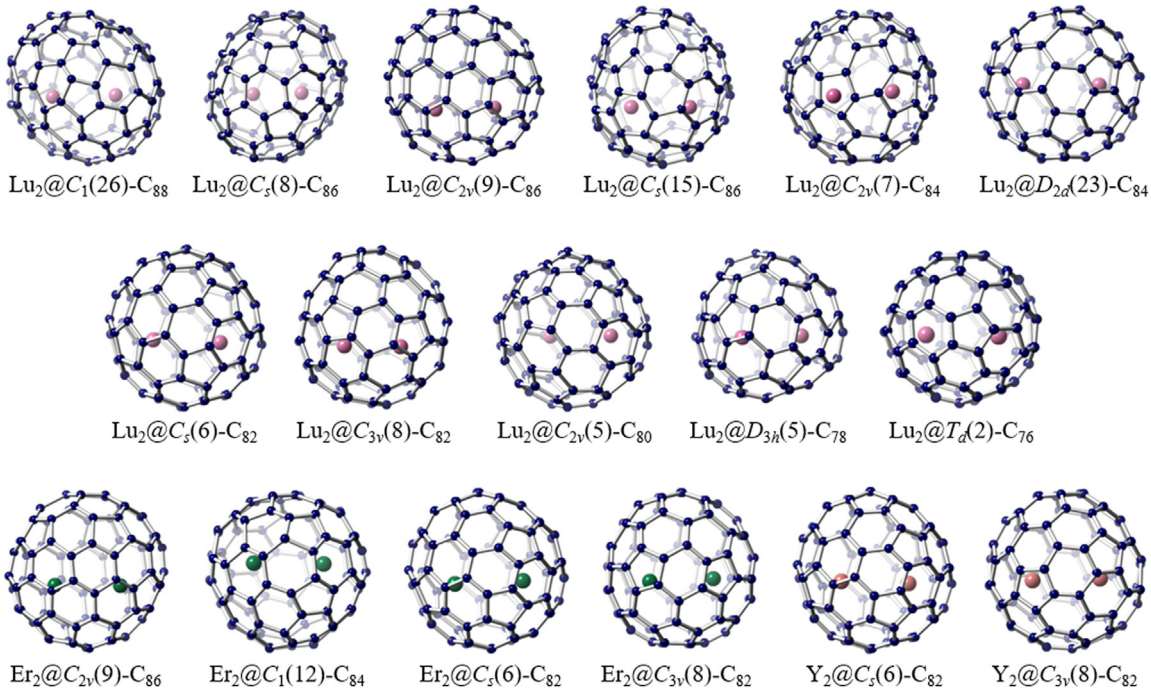

Fig. 5. Metal-metal bonding in pristine EMFs. Drawings show the single crystal X-ray structures of diverse $M_2@C_{2n}$-type (M = Lu, Er, and Y) dimetallofullerenes: $Lu_2@C_1(26)$-C_{88}, $Lu_2@C_s(8)$-C_{86}, $Lu_2@C_{2v}(9)$-C_{86}, $Lu_2@C_s(15)$-C_{86}, $Lu_2@C_{2v}(7)$-C_{84}, $Lu_2@D_{2d}(23)$-C_{84}, $Lu_2@C_s(6)$-C_{82}, $Lu_2@C_{3v}(8)$-C_{82}, $Lu_2@C_{2v}(5)$-C_{80}, $Lu_2@D_{3h}(5)$-C_{78}, $Lu_2@T_d(2)$-C_{76}, $Er_2@C_{2v}(9)$-C_{86}, $Er_2@C_1(12)$-C_{84}, $Er_2@C_s(6)$-C_{82}, $Er_2@C_{3v}(8)$-C_{82}, $Y_2@C_s(6)$-C_{82} and $Y_2@C_{3v}(8)$-C_{82}. The Lu atoms are highlighted in pink, the Er atoms are highlighted in green, and the Y atoms are highlighted in red.

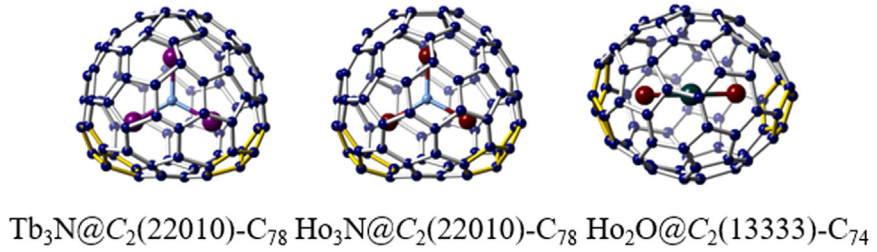

Fig. 6. Specific non-classical cage preferences. Single crystal X-ray examples of three novel cluster metallofullerenes: $Tb_3N@C_2(22{,}010)$-C_{78}, $Ho_3N@C_2(22{,}010)$-C_{78} and $Ho_2O@C_2(13{,}333)$-C_{74}. The Tb atoms are highlighted in purple, the Ho atoms are highlighted in claret-red, the N atoms are highlighted in blue, and the oxygen atom is highlighted in dark green. The fused-pentagons are highlighted in yellow.

tion of entrapped metal clusters. This diversity gives rise to unique properties in novel metallofullerenes that differ from those of conventional metallofullerenes. Presently, an extensive number of cluster metallofullerenes featuring non-IPR fullerene cage isomers have been discovered, unveiling their specific cage preferences for encapsulated unique metal clusters. For instance, the classical Sc_3N cluster favors an IPR $D_{3h}(5)$-C_{78} cage [43], whereas Ho_3N and Tb_3N clusters exhibit a preference for a non-IPR $C_2(22{,}010)$-C_{78} cage with two pairs of adjacent pentagons (Fig. 6) [74]. Computational and spectroscopic investigations have also revealed that $M_3N@C_{78}$ species with M = Y, Lu, La, Gd, Dy, and Tm exhibit the same preference for the $C_2(22{,}010)$-C_{78} cage [5]. Although significant non-IPR cage structures have been predicted for the Sc_2O cluster, the only isolated species is $Sc_2O@C_{70}$, which features a non-IPR $C_2(7892)$-C_{70} cage [75]. The predicted non-IPR cages for $Sc_2O@C_{2n}$, namely $C_s(10{,}528)$-C_{72} and $C_2(13{,}333)$-C_{74}, have not been experimentally observed. Remarkably, recent crystallographic analysis of various Ho_2O-containing EMFs unambiguously confirmed the adoption of an expanded configuration by the Ho_2O cluster within the non-IPR $C_2(13{,}333)$-C_{74} cage (Fig. 6), thus indicating the role of metal cluster compositions as influential templates of cage formation during the discharging process [76].

4.4. Transition metal-containing EMFs

Remarkably, within the realm of macroscopically synthesized EMFs over the past two decades, rare-earth metals, such as Group-3 elements (Sc, Y), and a majority of the lanthanide metals have been encapsulated within fullerene cages. This leads to an intriguing question regarding the possibility of forming EMFs with other elements in significant yields. The exploration of EMFs containing adjacent d-block transition metals was initiated in 1992 with the mass spectrometric detection of a titanium-only EMF, $Ti@C_{28}$, thereby expanding the scope of EMF investigations [77,78]. However, the macroscopic synthesis of Ti-containing EMFs (Ti_2C_{80} and Ti_2C_{84}) was first reported by Shinohara and colleagues [79,80], with subsequent studies theoretically determining their stable structures as $Ti_2C_2@C_{78}$ and $Ti_2C_2@C_{82}$, respectively [81,82]. Furthermore, in 2013, Echegoyen et al. successfully identified the first Ti-containing sulfide cluster metallofullerene, $Ti_2S@C_{78}$, where the cage exhibits $D_{3h}(5)$-C_{78} symmetry and the Ti_2S cluster demonstrates a near-linear structure [83]. More recently, Lu and co-workers achieved the preparation and structural characterization of a groundbreaking Ti-containing carbide cluster metallofullerene, $Ti_3C_3@I_h(7)$-C_{80} (Fig. 7) [84]. The internal C_3 unit displayed an anticipated cyclopropane-like

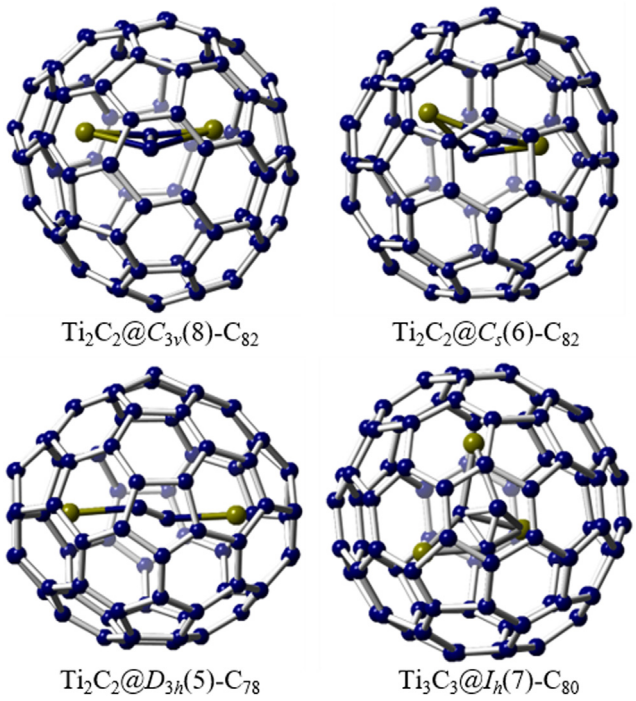

Fig. 7. The macroscopic synthesis of d-block transition metal-containing EMFs. Single crystal X-ray examples of four Ti-only cluster metallofullerenes: $Ti_2C_2@C_{3v}(8)$-C_{82}, $Ti_2C_2@C_s(6)$-C_{82}, $Ti_2C_2@D_{3h}(5)$-C_{78} and $Ti_3C_3@I_h(7)$-C_{80}. The Ti atoms are highlighted in olive green.

geometry, forming a novel perpendicular coordination with the Ti_3 unit. Notably, this unique coordination pattern, resembling cyclopropane, has never been observed in any reported organometallic complexes, providing novel insights into organo-transition metal chemistry. Subsequently, three Ti-containing CCMFs, namely $Ti_2C_2@D_{3h}(5)$-C_{78}, $Ti_2C_2@C_s(6)$-C_{82}, and $Ti_2C_2@C_{3v}(8)$-C_{82}, featuring an encapsulated Ti_2C_2 cluster within the carbon cages, were successfully isolated and characterized (Fig. 7) [85]. Single crystal X-ray analysis revealed that the Ti_2C_2 cluster adopted a stretched planar configuration within the smaller $D_{3h}(5)$-C_{78} cage, while a bent butterfly geometry was observed within the relatively larger $C_s(6)$-C_{82} and $C_{3v}(8)$-C_{82} cages. DFT calculations indicated that the anomalous geometric shapes of the Ti_2C_2 cluster in these carbide cluster metallofullerenes can be attributed to the varying number of electrons transferred from the Ti_2C_2 cluster to the cage, which is dependent on the size and electronic structure of the cage.

In addition to the limited instances of Ti-clusterfullerenes, an alternative approach involves utilizing Group-3 metals as the core to create versatile mixed-metal clusters in fullerene cages. When Ti was combined with Sc or Y and subjected to arc synthesis in the presence of nitrogen, the formation of nitride clusterfullerenes $TiM_2N@I_h(7)$-C_{80} (M = Sc, Y) was observed [86,87]. Furthermore, by employing a reactive gas atmosphere such as methane, Popov et al. identified the formation of a distinctive type of carbide clusterfullerenes, $TiM_2C@I_h(7)$-C_{80} (M = Sc, Y, Nd, Gd, Dy, Er, Lu), in which a Ti=C double bond was present (Fig. 8). This marked the first instance of EMFs featuring a multiple bond between the metal and the non-metal atom within the endohedral cluster [88–90].

However, the synthesis of V-only endohedral metallofullerenes has proven to be challenging. Unlike its neighbor Ti in the first 3d transition metal series, the encapsulation of pure vanadium species within the cage is quite difficult. In light of the mixed-metal strategy that yielded successful results in the synthesis of the M-Ti system, Sc was utilized to facilitate the encapsulation of V atoms. As a result, the first mixed-metal nitride cluster fullerenes containing vanadium, namely $VSc_2N@I_h(7)$-C_{80}, $V_2ScN@I_h(7)$-C_{80}, and $VSc_2N@D_{5h}(6)$-C_{80}, were successfully synthesized [91,92]. Subsequently, novel V-based trimetallic carbide cluster metallofullerenes, namely $VSc_2C@I_h(7)$-C_{80} and $VSc_2C_2@I_h(7)$-C_{80}, were also reported [93]. Similar to the mixed-metal Sc-Ti system, the presence of a V=C double bond was identified in $VSc_2C@I_h(7)$-C_{80}. However, the distance between V and C atoms in $VSc_2C_2@I_h(7)$-C_{80} corresponding to that of a typical single bond, as observed for conventional V-based organometallic complexes. Interestingly, in contrast to Ti-clusterfullerenes that typically encapsulate one Ti atom, V-containing clusters exhibit the potential to host either one or two V atoms within the fullerene cage, highlighting the sensitivity of the composition of non-Group-3 transition-metal-containing clusterfullerenes to the specific characteristics of the transition metal involved (Fig. 8).

4.5. Actinide metal-containing EMFs

In recent years, significant progress has been made in the synthesis and comprehensive investigation of actinide-based EMFs, uncovering distinct chemical bonding and coordination patterns that differ substantially from those observed in the rather extensively studied rare earth-based EMFs. Notably, the actinide elements, particularly uranium, exhibit variable oxidation states, in contrast with the relatively limited Ln^{2+}/Ln^{3+} oxidation states of the rare earth elements. This variation in oxidation states gives rise to new electronic structures and specific fullerene cage isomers to actinide EMFs. For instance, single crystal X-Ray diffractometric analyses and theoretical studies of monometallic uranium EMFs unveiled a cage isomer-dependent charge transfer phenomenon originating from the encapsulated uranium atom [94]. Furthermore, the considerably stronger interactions between the metal and the carbon cage in actinide EMFs have facilitated the stabilization of previously unexplored chiral non-IPR fullerene cage isomers, by providing these isomers in relatively high yields [95].

Recent investigations of uranium clusterfullerene families have unveiled the remarkable capability of fullerene cages to encapsulate diverse actinide clusters, showcasing important actinide bonding motifs achieved through electron transfer between the cluster and the carbon cage, as well as U-carbon coordination. Notably, the discovery of uranium metal cluster EMFs, such as $UCU@I_h(7)$-C_{80} and $UNU@I_h(7)$-C_{80}, represent the first examples of M_2C and M_2N clusters in the EMF field (Fig. 9) [96,97]. In $UCU@I_h(7)$-C_{80}, the combined experimental and theoretical investigations have shown a bent configuration featuring unsupported strong U=C covalent bonds for the U=C=U cluster and a formal oxidation state of 5+ for both uranium atoms. Similarly, an encapsulated U=N=U cluster has been stabilized within $U_2N@I_h(7)$-C_{80}, featuring an uncommon unsymmetrical structure characterized by two U=N bonds with uneven bond distances. Systematic investigations have indicated different oxidation states of +4 and +5 for the two uranium ions, with the f1/f2 population playing a dominant role in inducing distortion of the U=N=U cluster and resulting in the unsymmetrical structure. Further studies with $U_2X@I_h(7)$-C_{80} (X = C, N and O) have demonstrated that the number of U(f) electrons play a crucial role in controlling the symmetry of the U_2X cluster [97]. Notably, the U-X interaction in U=X=U clusters does not resemble classical multiple bonds, but rather resembles an anionic central ion X^{q-} with biased overlaps with the two metal ions, and this interaction weakens as the electronegativity of X increases. In addition, the crystallographic study of a mixed actinide-lanthanide cluster metallofullerene, $USc_2C@I_h(7)$-C_{80}, has revealed the shortest U=C double bond (2.011 Å) for U-containing EMFs to date. The U ion within the USc_2C cluster, located inside the $I_h(7)$-C_{80} cage, has an oxidation state of +4, resulting in a similar electronic structure to the previously reported $Ti^{4+}(Sc^{3+})_2C$ cluster [98].

Another interesting finding involves the stabilization of a U_2C_2 cluster within both the $I_h(7)$-C_{80} and $D_{3h}(5)$-C_{78} cages (Fig. 9) [99]. The C_2 units in both compounds exhibit unprecedented C≡C bonds, which are not observed in other carbide cluster metallofullerenes. Unlike the U=C covalent bonds observed in $UCU@I_h(7)$-C_{80}, the two U atoms in the

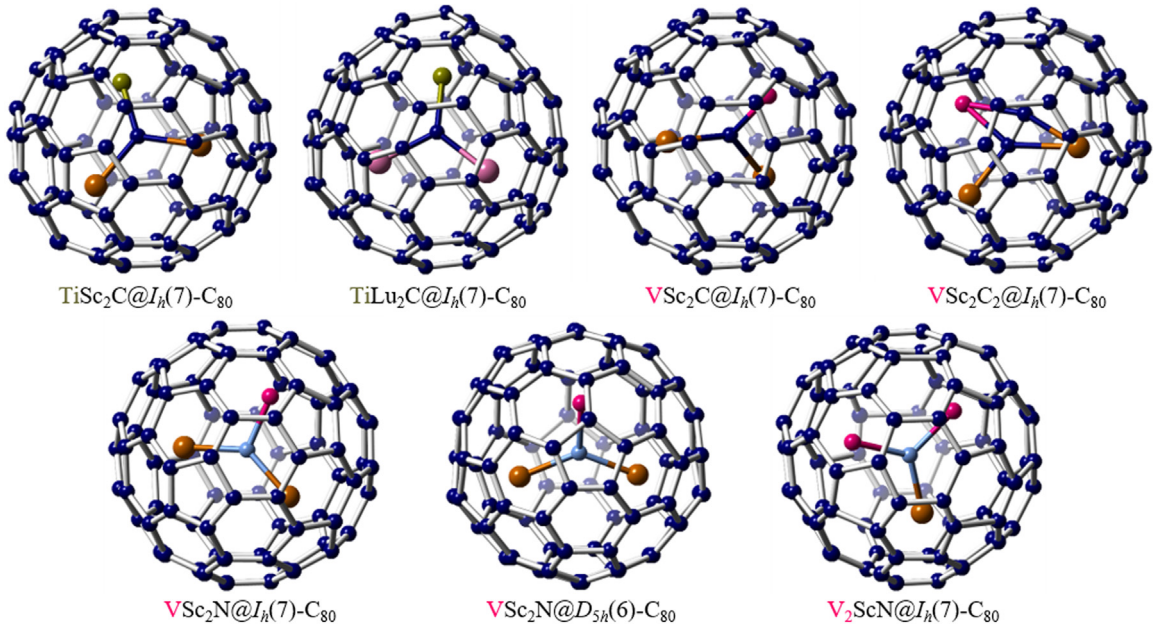

Fig. 8. The encapsulation of transition metals by using Group-3 metals as the core to create mixed-metal clusters. Single crystal X-ray examples of mixed-metal cluster fullerenes containing Ti or V: $TiSc_2C@I_h(7)$-C_{80}, $TiLu_2C@I_h(7)$-C_{80}, $VSc_2C@I_h(7)$-C_{80}, $VSc_2C_2@I_h(7)$-C_{80}, $VSc_2N@I_h(7)$-C_{80}, $VSc_2N@D_{5h}(6)$-C_{80} and $V_2ScN@I_h(7)$-C_{80}. The Ti atoms are highlighted in olive green, the V atoms are highlighted in fuchsia, the Lu atoms are highlighted in pink, the Sc atoms are highlighted in brown, and the N atoms are highlighted in blue.

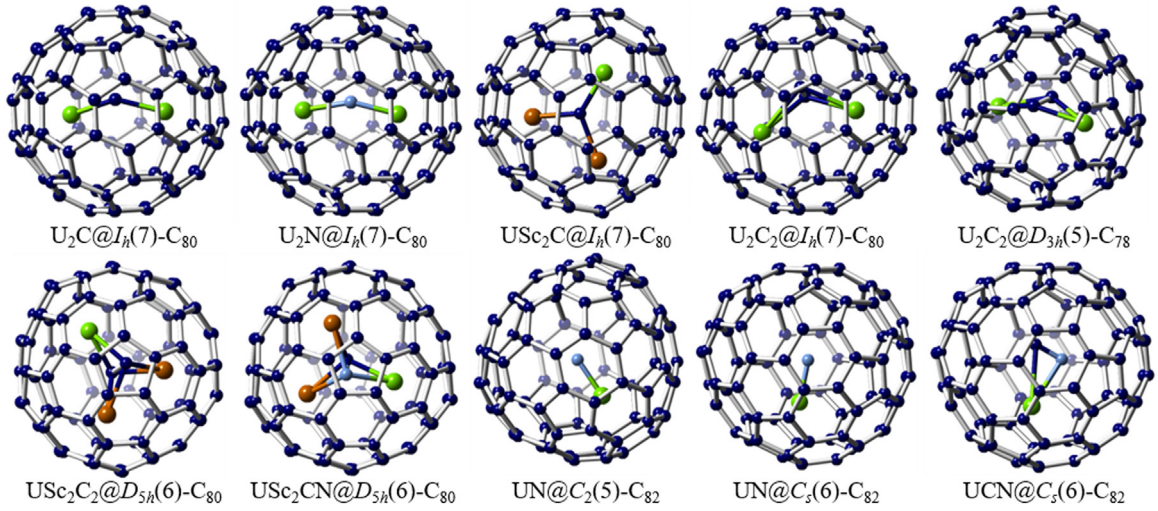

Fig. 9. The exploration of long-desired bonding features via the strong coordination interaction between uranium and non-metal atoms. Single crystal X-ray examples of U-containing cluster metallofullerenes: $U_2C@I_h(7)$-C_{80}, $U_2N@I_h(7)$-C_{80}, $USc_2C@I_h(7)$-C_{80}, $U_2C_2@I_h(7)$-C_{80}, $U_2C_2@D_{3h}(5)$-C_{78}, $USc_2C_2@D_{5h}(6)$-C_{80}, $USc_2CN@D_{5h}(6)$-C_{80}, $UN@C_2(5)$-C_{82}, $UN@C_s(6)$-C_{82} and $UCN@C_s(6)$-C_{82}. The U atoms are highlighted in light green, the Sc atoms are highlighted in brown, and the N atoms are highlighted in blue.

U_2C_2 cluster adopt a formal 4+ oxidation state, thus forming four predominantly ionic U-C bonds. Interestingly, despite the contrasting bonding interactions between $UCU@I_h(7)$-C_{80} and $U_2C_2@I_h(7)$-C_{80}, the U-U distances remain essentially consistent in both compounds. Subsequent investigations have further unveiled a variety of bonding motifs exhibited by uranium, exemplified by the successful synthesis and characterization of $UCN@C_s(6)$-C_{82}, $USc_2C_2@D_{5h}(6)$-C_{80}, $USc_2CN@D_{5h}(6)$-C_{80}, $UN@C_s(6)$-C_{82} and $UN@C_2(5)$-C_{82}, (Fig. 9) [100–102]. For instance, the UCN cluster, with a triangular configuration, exhibits an open-shell electronic structure $[UCN]^{2+}@[C_s(6)\text{-}C_{82}]^{2-}$, with uranium adopting a + 3 oxidation state. In addition, the presence of a U≡N bond in the UN cluster, along with uranium displaying a formal oxidation state of +5, has been confirmed through another study with $UN@C_s(6)$-C_{82} and $UN@C_2(5)$-C_{82}. These findings provide evidence for the electronic structure of $(UN)^{2+}@(C_{82})^{2-}$. Furthermore, it has been observed that U≡N is immobilized and coordinated to the fullerene cage at 100 K, while rotational movement within the cage is observed at 273 K. Likewise, the electronic configurations of $USc_2C_2@D_{5h}(6)$-C_{80} and $USc_2CN@D_{5h}(6)$-C_{80} have revealed intriguing donation bonding features, characterized by novel U-C partial triple bond characteristics and multicenter bonding expansion across the Sc centers. Of particular note, different oxidation states of +6 and +5 were confirmed for the U ions in $USc_2C_2@D_{5h}(6)$-C_{80} and $USc_2CN@D_{5h}(6)$-C_{80}, respectively. The exploration of novel uranium clusters with unprecedented bonding motifs and intriguing electronic structures not only offers valuable insights into the field of coordination chemistry and fundamental actinide bonding properties,

but also broadens our knowledge of the interactions of actinide clusters within fullerene frameworks, opening up new avenues for future research in this intriguing area.

5. Improved understanding in the formation mechanism of EMFs

To date, the precise mechanisms underlying the formation of EMFs have remained elusive, impeded by the acquisition of direct experimental evidence. Although two distinct theoretical models proposing top-down and bottom-up processes have been put forward [103,104], recent investigations have focused on elucidating the specific formation mechanisms of EMFs synthesized under varying arcing conditions. The controlled synthesis studies of europium-containing EMFs have shed light on the prevalent formation of Eu@$C_{74–88}$ while observing the scarcity of Eu_2@C_{2n} and Eu_3@C_{2n} species [105]. In order to comprehend the underlying factors governing the preferential formation of mono-EMFs, calculations have been employed, introducing a novel concept known as encapsulation energy (E_e) to quantify the feasibility of EMF formation. A higher E_e value corresponds to a greater likelihood of EMF formation [106], thus offering new insights into the formation mechanism of EMFs. In an alternative line of investigation, the synthesis and structural characterization of a carbide cluster metallofullerene featuring an unprecedented heptagonal ring, namely Sc_2C_2@C_s(hept)-C_{88}, have provided substantial experimental evidence supporting the bottom-up growth model [107]. It has been proposed that this non-classical carbide cluster endohedral represents a kinetically trapped intermediate formed via a direct C_2 insertion in the bottom-up growth process originating from Sc_2C_2@C_{2v}(9)-C_{86}. Although Sc_2C_2@C_s(hept)-C_{88} may not be thermodynamically favored, Sc_2C_2@C_{2v}(9)-C_{86} is proposed to be more stable from a thermodynamic standpoint [108], revealing an important pathway for capturing non-classical EMFs through C_2 insertion. Given the relatively low energy barrier associated with C_2 insertion (approximately 2 eV), an intriguing question arises as to whether it is possible to generate novel EMFs via single carbon atom insertion (C_1 insertion). To address this question, a C_1 implantation mechanism was proposed based on the synthesis and crystallographic characterization of VSc_2C@I_h(7)-C_{80} and VSc_2C_2@I_h(7)-C_{80} [93]. The C_1 implantation process can be divided into two distinct steps: the bonding process (C_1 insertion) and the self-driven encapsulation process. The energy barrier associated with C_1 implantation (3.95 eV) is slightly higher than that of C_2 insertion (~2 eV), yet considerably lower than that of the Stone-Wales transformation (~7 eV), thereby indicating the feasibility of C_1 implantation under high temperatures generated by the arc-discharging process. Notably, detailed theoretical investigations confirm that the high likelihood of the transition from VSc_2C to VSc_2C_2 can be attributed to the presence of an unpaired electron on the vanadium atom, which exhibits a strong affinity for electron pairing with carbon radicals. This investigation into the mechanism of C_1 implantation provides the first mechanistic link elucidating the evolution of endohedral metal-carbon clusters during the formation process of EMFs.

The structural identification of various endohedral metallofullerenes has paved the way for comprehensive investigations concerning the inter-cage transformations among existing fullerene cages, which make it possible to establish typical transformation routes to offer valuable insights into the formation mechanism of EMFs. A recent study focusing on uranium EMFs possessing non-IPR chiral carbon cages, namely U@C_1(17,418)-C_{76} and U@C_1(17,894)-C_{80}, revealing a novel structural rearrangement pathway indicative of a bottom-up growth process [95]. Specifically, enantiomer e1 (e2) of C_1(17,418)-C_{76} and enantiomer e2 (e1) of C_1(17,894)-C_{80} were found to be topologically connected through two C_2 insertions without the need of Stone-Wales rearrangements. These pathways exhibit lower energy demands compared to those preserving the same chirality, thus providing new mechanistic insights into the formation of metallofullerenes during arc discharging processes. In a consistent manner, the interconversion map for all characterized EMFs was expanded by capturing several key cages, including U@C_1(17,418)-C_{76}, U@C_1(28,324)-C_{80}, U@C_1(11)-C_{86}, Eu@C_2(27)-C_{88}, Gd_2C_2@C_1(51,383)-C_{84} and La_2C_2@C_2(816)-C_{104} [105,109-111]. These low-symmetry fullerene cages serve as starting points for fullerenes with either IPR or non-IPR cages through diverse transformation routes. Notably, the topological analysis reveals that C_1(17,418)-C_{76}, C_1(11)-C_{86}, and C_2(27)-C_{88} can be obtained through spontaneous rolling and wrapping directly from flat graphene sheets, consistent with observations from transmission electron microscopy (TEM) visualizations of fullerene formation from graphene sheets [112]. Additionally, it is worth noting that fullerene structural interconversion maps provide evidence for the simultaneous occurrence of both top-down and bottom-up processes during arc discharging. Certain asymmetric intermediates, such as C_1(28,324)-C_{80}, can serve as precursors for the formation of larger cages in growth processes or smaller cages in shrinking routes.

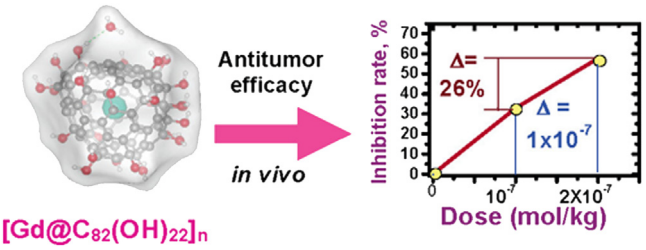

Fig. 10. Biomedical applications based on water-soluble derivatives of Gd-EMFs. The very high antineoplastic efficiency of Gd@C_{82}(OH)$_{22}$ nanoparticles with an average size of approximately 22 nm against H_{22} hepatoma in mice [113]. Copyright 2005, American Chemical Society.

6. New achievements in the application of EMFs

The distinctive electronic structures and innovative bonding motifs exhibited by the encapsulated metal moieties, coupled with their remarkable interactions with the carbon cage, render EMFs as promising candidates for the fabrication of molecular materials with diverse applications. As the mass production of EMFs has reached significant quantities, extensive research efforts have been devoted to exploring their practical applications and uncovering their new functionalities. In this section, we will primarily discuss the recent advancements in the field of functional metallofullerene materials, with a particular focus on their applications in nanomedicine, single-molecule magnets, and electronic devices. These areas represent key domains where EMFs have demonstrated potential for significant applications and have witnessed notable progress in recent years.

6.1. Biomedical applications

The inherent non-toxicity of the carbon cage and its ability to provide a totally isolated environment for the internal metal species make water-soluble derivatives of metallofullerenes promising candidates for medical diagnosis and therapy. One notable example is the utilization of water-soluble derivatives of Gd-containing EMFs, which have demonstrated significant potential as advanced contrast agents for magnetic resonance imaging (MRI). This is attributed to the presence of seven unpaired f-electrons in Gd^{3+}, which give rise to super-paramagnetic properties. Similarly, a series of metallofullerenes containing Lu_3N clusters have been successfully employed as X-ray contrast agents, leveraging the large cross-section of the Lu atom [43].

It is noteworthy to highlight that nanoparticles of [Gd@C_{82}(OH)$_{22}$]$_n$ have also demonstrated potential antitumor activity (Fig. 10). In 2005, Zhao et al. conducted a study showcasing the potent antineoplastic effects of Gd@C_{82}(OH)$_{22}$ nanoparticles with an average size of approximately 22 nm against H_{22} hepatoma in mice [113]. Remarkably, these nanoparticles exhibited superior anticancer efficacy compared to the

clinical anticancer drug paclitaxel, while showing minimal side effects. The proposed mechanism of action for $Gd@C_{82}(OH)_{22}$ involves the indirect inhibition of tumor growth in human pancreatic cancer xenografts in a nude mouse model [114]. In addition, $Gd@C_{82}(OH)_{22}$ nanoparticles have been found to significantly suppress cancer metastasis in aggressive and invasive human breast cancer models by inhibiting matrix metalloproteinase production, rather than exerting direct cytotoxicity [115]. Notably, while extensive research has focused on the anticancer properties of $[Gd@C_{82}(OH)_{22}]_n$ nanoparticles, Wang and colleagues reported a novel water-soluble $Gd@C_{82}$ particles modified with amino acids, denoted as $(Gd@C_{82})_m(OH)_n(Ala)_x$, which exhibited exceptional antitumor effects in mice implanted with H_{22} hepatoma [116]. These $(Gd@C_{82})_m(OH)_n(Ala)_x$ particles, with an average size of approximately 127.7 nm, demonstrated superior therapeutic efficacy by rapidly disrupting tumor blood vessels under radiofrequency (RF) irradiation, surpassing the performance of $(Gd@C_{82})_m(OH)_n$. Furthermore, Wang and colleagues introduced an unprecedented tumor vascular-targeting therapeutic technique for cancers, utilizing $(Gd@C_{82})_m(OH)_n$ nanoparticles with an average diameter of approximately 140 nm and applying radiofrequency (RF) irradiation (200 MHz) for 30 min [117]. The proposed mechanism involves the accumulation of $(Gd@C_{82})_m(OH)_n$ nanoparticles in the nanogaps between endothelial cells, leading to the specific destruction of tumor blood vessels. Subsequent investigations revealed that the therapeutic technique using $(Gd@C_{82})_m(OH)_n$ leads to down-expression of tumor vascular endothelial cadherin (VE-cadherin) [118], causing disruption of blood flow and tumor necrosis.

Notably, $Gd@C_{82}(OH)_{22}$ nanoparticles have also been shown to regulate oxidative stress in tumor cells in vivo and function as scavengers of reactive oxygen species (ROS), contributing to their antitumor activity. Wang and colleagues reported the therapeutic potential of $(Gd@C_{82})_m(OH)_n$ nanoparticles in protecting oxidative injury during chemotherapy. These nanoparticles have demonstrated remarkable radical scavenging activity, thereby effectively mitigating damage induced by cyclophosphamide chemotherapy [119]. Furthermore, a water-soluble derivative of $Gd@C_{82}$, modified with multiple ethylenediamine (EDA) groups and referred to as $Gd@C_{82}$-$(EDA)_8$, has been demonstrated to possess hydroxyl radical scavenging properties [120]. This derivative exhibited a cytoprotective effect by mitigating H_2O_2-induced injuries in human epidermal keratinocytes-adult (HEK-a) cells.

6.2. Single molecular magnets

Metallofullerenes possess unique electronic structures and internal metal atoms that give rise to diverse magnetic properties, holding great promise in various applications such as quantum information processing (QIP), memory and logic devices, medical imaging, and single-molecule magnets (SMMs) [121]. In 2012, Greber and colleagues made a significant breakthrough by discovering slow magnetic relaxation in $DySc_2N@I_h(7)$-C_{80}, exhibiting a magnetic blocking temperature (T_B) of up to 7 K. This discovery sparked the exploration of the SMM properties of metallofullerenes containing lanthanide ions [122]. The fullerene cages in metallofullerenes act as nano-containers, providing stabilization for unconventional metal cluster configurations and protection against ambient conditions. The combination of their unique physicochemical properties, the varied structures of encapsulated magnetic species, and the potential to create functional devices, offers opportunities for creating well-controlled and high-performance SMMs for practical applications.

Recent advancements in the field have primarily focused on exploring the single-molecule magnetism of Dy-containing EMFs. Due to the presence of high thermal barriers, Dy-containing EMFs exhibit the potential for achieving remarkably high magnetic blocking temperatures and significantly prolonged magnetic lifetimes at low temperatures. However, in most cases, the existence of quantum tunneling of magnetization (QTM) will lead to a plateau in magnetic relaxation lifetimes at low temperatures, thereby placing limitations on the performance of Dy-EMF SMM. Intriguingly, in contrast to $DySc_2N@I_h(7)$-C_{80}, a dilanthanide clusterfullerene, $Dy_2ScN@I_h(7)$-C_{80}, demonstrated magnetic hysteresis and magnetization blocking at 8 K, without exhibiting QTM [123]. Recent magnetic investigations have further revealed that the magnetization relaxation and blocking temperature in $DyM_2N@I_h(7)$-C_{80} (M = Sc, Y, Lu) are related to the mass of M, while the magnetic behavior of $Dy_2MN@I_h(7)$-C_{80} (M = Sc, Y, La, Lu) are associated with varied Dy…Dy coupling caused by the size of M^{3+} ions [124]. Significantly, the presence of ferromagnetic coupling between the two Dy spins suppresses the occurrence of zero-field QTM, while simultaneously creating new relaxation pathways that result in a relaxation rate reliant on the strength of the coupling. Consequently, recent studies in EMF SMMs have primarily focused on systems containing two Dy ions. For instance, $Dy_2O@C_{3v}(8)$-C_{82} exhibits a relatively high magnetization blocking temperature of 7.4 K [125], comparable to that of $Dy_2ScN@I_h(7)$-C_{80}. Notably, $Dy_2O@C_s(10{,}528)$-C_{72}, $Dy_2O@C_2(13{,}333)$-C_{74}, $Dy_2O@C_s(6)$-C_{82}, $Dy_2O@C_{2v}(9)$-C_{82}, $Dy_2S@C_{3v}(8)$-C_{82}, and $Dy_2ScN@D_{5h}(6)$-C_{80} show hysteresis in the range of 4–6 K [125–128], while carbide clusterfullerenes such as $Dy_2TiC@I_h(7)$-C_{80}, $Dy_2TiC_2@I_h(7)$-C_{80}, and $Dy_2C_2@C_s(6)$-C_{82} exhibit hysteresis of magnetization below 2 K [88,127].

The establishment of di-metallofullerenes (di-EMFs) with a covalent metal-metal bond represents an elegant approach to enhance the magnetic coupling between ions. The formation of metal-metal bonds leads to substantial exchange interactions within magnetic molecules, thereby offering significant advantages for molecular magnetism. In 2017, Popov et al. reported the synthesis of an exceptional single molecule magnet $Dy_2@I_h(7)$-$C_{80}(CH_2Ph)$ with a notable blocking temperature of magnetization at 21.9 K, exhibiting hysteresis in the temperature range of 1.8 to 21 K [69]. In this system, $Dy_2@I_h(7)$-$C_{80}(CH_2Ph)$ can be regarded as a three-spin system [Dy^{3+}-e-Dy^{3+}], where the ferromagnetic coupling between the two Dy^{3+} ions is facilitated through the electron spin interaction. Theoretical calculations indicate that the negatively charged electron between the Dy^{3+} ions mediates a strong ferromagnetic exchange between the radical Dy-Dy bond, while the direct antiferromagnetic coupling between the Dy^{3+} ions is negligible. Subsequent investigations on a series of $M_2@I_h(7)$-$C_{80}(CH_2Ph)$ compounds (M = Y, Gd, Dy, Tb, Ho, Er, etc.) with an electron spin positioned between two magnetic ions revealed that the presence of a high-spin magnetic ground state resulting from strong ferromagnetic exchange coupling, in conjunction with single-ion anisotropy and collinearity of lanthanide spins, played pivotal roles in achieving excellent SMM behavior [129]. Particularly noteworthy is the observation that $Tb_2@I_h(7)$-$C_{80}(CH_2Ph)$ exhibits a substantial coercivity and an impressively high blocking temperature of 29 K, accompanied by broader hysteresis and a longer relaxation time for QTM reaching 18 h. However, the specific shape of the 4f charge density associated with a different lanthanide element would result in the variation in magnetic anisotropy of these M_2 dimers. For instance, Ho_2, with mixed single-ion ligand-field (LF) states and tilted magnetic moments, exhibits only modest SMM behavior, while Er_2, possessing an easy-plane single-ion anisotropy, does not demonstrate significant SMM properties (Fig. 11).

As previously mentioned, the M_2 dimers incorporated into $M_2@I_h(7)$-C_{80} (M = Y, Gd, Dy, Tb, etc.) contribute five electrons to the cage, resulting in a single-electron-occupied M-M bond with a formal oxidation state of +2.5 on each metal ion. Two approaches have been explored to stabilize these unstable radicals. The first involves the formation of radical monoadducts through functionalization of the cage with a radical group such as CF_3 or benzyl. The second approach entails substituting a carbon atom in the cage with a nitrogen atom, yielding azafullerenes known as $M_2@I_h(7)$-$C_{79}N$ (M = Tb, Gd…). Notably, the absence of functional groups in $M_2@I_h(7)$-$C_{79}N$ would enhance its thermal stability and facilitate the growth of thin molecular films through sublimation. In 2019, it was discovered that azafullerene $Tb_2@I_h(7)$-

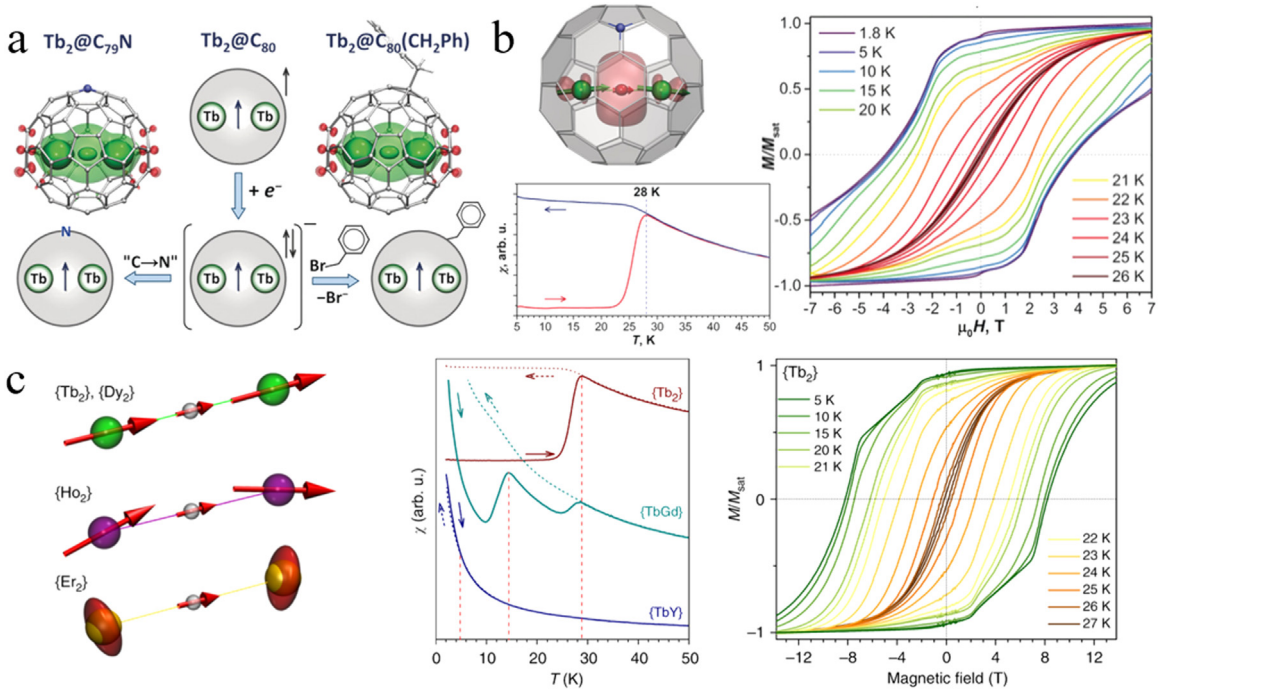

Fig. 11. High-performance metallofullerene single molecular magnets. The comparison of the SMM properties between $Tb_2@I_h(7)$-$C_{79}N$ and $Tb_2@I_h(7)$-$C_{80}(CH_2Ph)$ [129,130]. (a) The spin density distributions in $Tb_2@I_h(7)$-$C_{79}N$ and $Tb_2@I_h(7)$-$C_{80}(CH_2Ph)$. (b) The alignment of magnetic moments of Tb_2 dimers in $Tb_2@I_h(7)$-$C_{79}N$, as well as the magnetic hysteresis curves and blocking temperature of magnetization for $Tb_2@I_h(7)$-$C_{79}N$. (c) The alignment of magnetic moments of M_2 dimers in a series of $M_2@I_h(7)$-$C_{80}(CH_2Ph)$ compounds (M = Tb, Dy, Ho and Er), as well as the magnetic hysteresis curves and blocking temperature of magnetization for $Tb_2@I_h(7)$-$C_{80}(CH_2Ph)$. Copyright 2019, Springer Nature. Copyright 2019, Wiley-VCH Verlag GmbH & Co. KGaA.

$C_{79}N$ exhibits SMM behavior with a high blocking temperature of 27 K and a significant electron-Tb exchange coupling constant (Fig. 11) [130]. This prompts an interesting comparison of the SMM properties between $Tb_2@I_h(7)$-$C_{79}N$ and $Tb_2@I_h(7)$-$C_{80}(CH_2Ph)$, as they possess identical spin systems encapsulated within the same fullerene cage, but with different stabilization protocols. Significantly, the considerable variation in the electrostatic potential (ESP) distribution exhibited by $Tb_2@I_h(7)$-$C_{79}N$ results in a tilting of the magnetic moments of the Tb ions by approximately 7° away from the Tb-Tb bond. Conversely, in $Tb_2@I_h(7)$-$C_{80}(CH_2Ph)$, the magnetic moments of the Tb ions remain aligned along the Tb…Tb axis due to a less pronounced variation in the ESP.

6.3. Single-metallofullerene devices

In response to the growing demands for data-driven applications, such as machine learning, in-memory computing presents a promising approach by integrating logic operations and data storage. Various macroscopic non-volatile memory devices, including resistive switching random access memory, phase-change memory, magnetoresistive random access memory, and ferroelectric random access memory, have demonstrated the feasibility of logic-in-memory operations [131–134]. In order to achieve greater miniaturization of electronic devices and enhance their power efficiency, researchers have demonstrated the operation of molecular-scale non-volatile memory devices, including self-assembled monolayers and molecular thin films, at remarkably low operating voltages below 1.0 V. Consequently, it suggests that single-molecule non-volatile memory devices could serve as a potential ultimate solution for realizing logic-in-memory computing. In this regard, the manipulation of spin or electric dipole has been recognized as a promising approach for achieving single-molecule scale in-memory logic operations. Recently, a gate-controlled three-terminal device based on $Gd@C_{82}$ has demonstrated low-temperature single electric dipole bistability below 1.6 K [135]. However, achieving single electric dipole bistability at room temperature remains challenging due to the inherent difficulties associated with effectively controlling random molecular orientations.

EMF molecules have gained attention due to their ability to attain room-temperature single electric dipole bistability. This is attributed to their capacity to modulate single permanent dipoles that reside within the fullerene cages. Theoretical calculations have also played a crucial role in elucidating the appropriateness of the encapsulation energy and chemical bonding energy between a Sc^{3+} ion and the fullerene cage, thereby confirming their potential for achieving room-temperature switching [136]. Very recently, logic-in-memory operations based on the manipulation of a single electric dipole, were successfully demonstrated by Xie and co-authors for $Sc_2C_2@C_s$(hept)-C_{88} (Fig. 12) [137]. It is noteworthy that this endohedral exhibits distinguishable electrical read-out signals due to its favorable room-temperature stability and asymmetry resulting from the presence of the unique heptagonal ring. Furthermore, the disordered Sc_2C_2 cluster possesses a quasi-permanent dipole, enabling its rotation within the cage under the influence of an applied electric field. The application of a low voltage range of ±0.8 V to the single-metallofullerene junction enabled the reversible encoding and storage of digital information through controlled manipulation of the independent permanent dipole of Sc_2C_2 within the C_s(hept)-C_{88} cage. As a result, 14 distinct Boolean logic functions were experimentally implemented in the single-$Sc_2C_2@C_s$(hept)-C_{88} devices (Fig. 12). In-depth theoretical findings show that the origin of the non-volatile memory behavior stems from the reorientation of the Sc_2C_2 group's dipole within the fullerene cage, induced by an applied electric field. In addition, the presence of non-volatile memory characteristics in another two carbide cluster metallofullerenes, namely $Sc_2C_2@D_{2d}(23)$-C_{84} and $Sc_2C_2@C_{2v}(9)$-C_{86}, suggests that EMFs with an enclosed single dipole group hold great promise as potential candidates for the design of single-molecule binary logic-in-memory devices. This pioneering demonstration marks a significant advancement in the development of room-temperature electrically controlled in-memory logic devices,

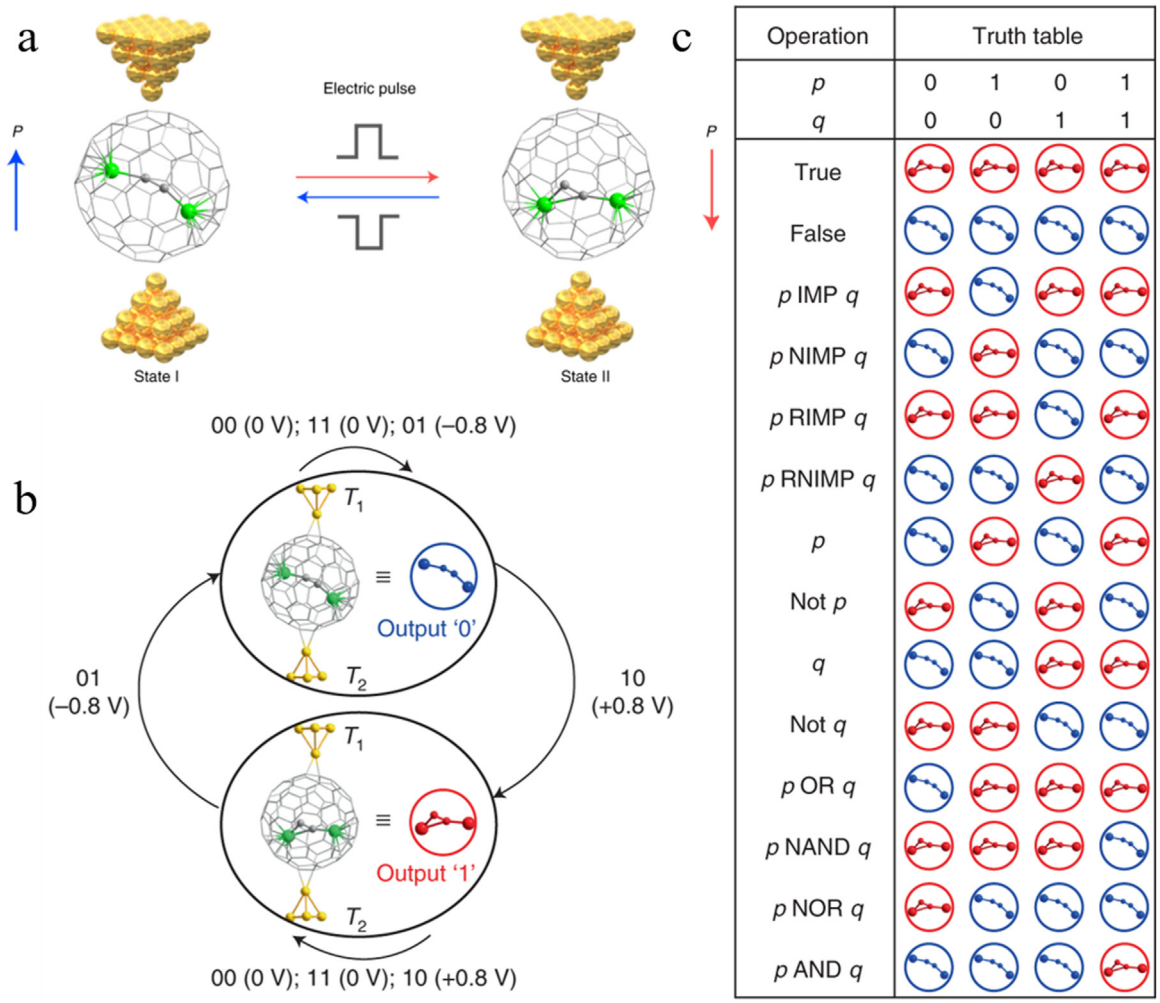

Fig. 12. Room-temperature logic-in-memory single-metallofullerene ($Sc_2C_2@C_s$(hept)-C_{88}) device [137]. (a) Different single $Sc_2C_2@C_s$(hept)-C_{88} junction configurations when states I and II are embedded in two-terminal gold electrodes. (b) Logic operations of the single-metallofullerene device. (c) The truth table of 14 fundamental Boolean logic functions implemented in the single-$Sc_2C_2@C_s$(hept)-C_{88} devices. Copyright 2022, Springer Nature.

paving the way for the development of nanoelectronic devices for in-memory computing.

7. Conclusion and perspective

Endohedral metallofullerenes provide an exceptional platform for the exploration of the distinctive structures and properties of metallic species that are not attainable in conventional systems outside the confinement of fullerene cages. However, the development of novel EMFs is significantly hindered by challenges associated with their synthesis and purification. In contrast to the conventional arc-discharge method, which yields EMFs in low quantities within the carbon soot, the combustion method provides novel insights into the macroscopic synthesis of desired EMF species, particularly those with non-classical cage structures. Alternatively, the development of purification protocols that circumvent the need for HPLC process, such as supramolecular purification strategies utilizing nanocapsules, offers an effective approach for selectively capturing specific EMF compounds. To date, various types of metallofullerenes have been successfully synthesized and isolated. The diversity of the encapsulated metal species gives rise to new structures and distinct properties. Firstly, intriguing phenomena related to the bonding inside and outside the fullerene cages have been observed, providing fresh insights into coordination chemistry. On one hand, a surprising regioselective dimerization process is observed for a pair of paramagnetic mono-EMFs, specifically M@C_{82} (M = Y, Er, Ce), through simple co-crystallization with Ni^{II}(OEP), indicating a bonding behavior influenced by spin interactions. On the other hand, direct metal-metal bonding is detected between the two M^{2+} ions (M = Lu, Y, Er) in the resulting di-EMFs, offering valuable knowledge regarding the coordination interactions between metals and carbon elements. Secondly, the encapsulation of transition metals (Ti, V) and actinide metals (Th, U) into fullerene cages holds significant importance as their strong coordination ability to interact with non-metal atoms (C, N, O, S) would stimulate research into the formation of new metal clusters with desired bonding features that researchers have been seeking for a considerable period of time. Various examples have been presented, such as the formation of unexpected C_3-rings with cyclopropane-like geometry, C≡C triple bonds, M=X double bonds (where M = Ti, V, U, Th and X = C, N, O), and U≡N triple bonds. Thirdly, the ongoing exploration of these novel EMF structures holds the promise of bridging the existing gaps in the proposed growth maps, ultimately yielding substantial evidence that establishes a reliable growth mechanism for EMFs. Enhanced understanding of the formation mechanism for EMFs will lead to further optimization of synthetic protocols, resulting in higher yields and the discovery of novel structures with unique properties. Last but not least, the exceptional electronic structures of the internal metal moieties and their remarkable interactions with the fullerene cage give rise to multifunctional properties, paving the way for promising applications of

EMFs in a wide range of fields, including biomedicine, single-molecule magnets, electronic devices.

Significantly, recent advancements in the field of fullerenes offer a fresh perspective in the realm of designing high-performance electrocatalysts, such as the Pt/C_{60} single-atom catalyst and the C_{60}_Cu/SiO_2 catalyst. These breakthroughs point towards a novel approach to surmount the limitations faced by conventional catalysts. Furthermore, the successful synthesis of polymeric fullerene layers exhibiting intriguing electronic and magnetic properties opens up avenues for potential applications in transistors, energy storage devices, superconductors, confined light systems, and quantum-materials-based devices. The development of functionalized fullerene complexes will also offer new perspectives into the application of fullerenes in the field of next-generation batteries. A notable example is the incorporation of nitro groups into the C_{60} cage, resulting in nitrofullerenes [138]. These nitrofullerenes exhibit excellent compatibility with various electrolytes, thereby serving as effective additives that greatly enhance the reversible and electrochemical performance of sodium metal batteries. Likewise, a recently introduced C_{60}-S supramolecular complex, featuring high-density active sites for the adsorption and electrochemical conversion of lithium polysulfides (LiPSs), was applied as a stable cathode material for high-performance lithium-sulfur batteries.[139] In line with this trajectory, there is high anticipation for the invention of a new generation of EMF-based catalysts, EMF electrolyte additives, EMF-S cathodes and EMF functional materials. The ongoing exploration of their molecular devices, characterized by unprecedented properties due to the existence of metal moieties, holds the potential to unveil a vast realm of boundless opportunities across diverse applications.

Declaration of competing interest

The authors declare that they have no conflicts of interest in this work.

Acknowledgments

Financial support from National Natural Science Foundation of China (22201227, 21925104, 92261204) and Qin Chuang Yuan Program of Shaan Xi Province (2021QCYRC4-37) is greatly acknowledged. L. E. thanks the Robert A. Welch Foundation (AH-0033) for an endowed chair and the U.S. NSF (CHE-1801317) for generous financial support.

References

[1] H.W. Kroto, J.R. Heath, S.C. O'Brien, et al., C_{60}: Buckminsterfullerene, Nature 318 (6042) (1985) 162–163.
[2] A. Hirsch, et al., The era of carbon allotropes, Nat. Mater. 9 (2010) 868–871.
[3] X. Lu, L. Feng, T. Akasaka, et al., Current status and future developments of endohedral metallofullerenes, Chem. Soc. Rev. 41 (23) (2012) 7723–7760.
[4] S. Yang, F. Liu, C. Chen, et al., Fullerenes encaging metal clusters-clusterfullerenes, Chem. Commun. 47 (43) (2011) 11822–11839.
[5] A.A. Popov, S. Yang, L. Dunsch, et al., Endohedral fullerenes, Chem. Rev. 113 (8) (2013) 5989–6113.
[6] J.R. Heath, S.C. Obrien, Q. Zhang, et al., Lanthanum complexes of spheroidal carbon shells, J. Am. Chem. Soc. 107 (25) (1985) 7779–7780.
[7] Y. Chai, T. Guo, C.M. Jin, et al., Fullerenes with metals inside, J. Phys. Chem. 95 (20) (1991) 7564–7568.
[8] R.D. Johnson, M.S. de Vries, J. Salem, et al., Electron paramagnetic resonance studies of lanthanum-containing C_{82}, Nature 355 (6357) (1992) 239–240.
[9] W. Cai, C.-H. Chen, N. Chen, et al., Fullerenes as nanocontainers that stabilize unique actinide species inside: Structures, formation, and reactivity, Acc. Chem. Res. 52 (7) (2019) 1824–1833.
[10] A.K. Geim, K.S. Novoselov, et al., The rise of graphene, Nat. Mater. 6 (3) (2007) 183–191.
[11] Q.H. Wang, K. Kalantar-Zadeh, A. Kis, et al., Electronics and optoelectronics of two-dimensional transition metal dichalcogenides, Nat. Nanotech. 7 (11) (2012) 699–712.
[12] L. Li, Y. Yu, G.J. Ye, et al., Black phosphorus field-effect transistors, Nat. Nanotech. 9 (5) (2014) 372–377.
[13] K.S. Novoselov, A.K. Geim, S.V. Morozov, et al., Electric field effect in atomically thin carbon films, Science 306 (5696) (2004) 666–669.
[14] Q. Fan, L. Yan, M.W. Tripp, et al., Biphenylene network: A nonbenzenoid carbon allotrope, Science 372 (6544) (2021) 852–856.
[15] M. Kolmer, A.K. Steiner, I. Izydorczyk, et al., Rational synthesis of atomically precise graphene nanoribbons directly on metal oxide surfaces, Science 369 (6503) (2020) 571–575.
[16] H. Yu, Y. Xue, Y. Li, et al., Graphdiyne and its assembly architectures: Synthesis, functionalization, and applications, Adv. Mater. 31 (42) (2019) 1803101.
[17] P.V. Bakharev, M. Huang, M. Saxena, et al., Chemically induced transformation of chemical vapour deposition grown bilayer graphene into fluorinated single-layer diamond, Nat. Nanotech. 15 (1) (2020) 59–66.
[18] C.T. Toh, H. Zhang, J. Lin, et al., Synthesis and properties of free-standing monolayer amorphous carbon, Nature 577 (7789) (2020) 199–203.
[19] T.L. Makarova, B. Sundqvist, R. Höhne, et al., Magnetic carbon, Nature 413 (6857) (2001) 716–718.
[20] C.H. Xu, G.E. Scuseria, et al., Theoretical predictions for a two-dimensional rhombohedral phase of solid C_{60}, Phys. Rev. Lett. 74 (2) (1995) 274–277.
[21] S. Okada, S. Saito, et al., Electronic structure and energetics of pressure-induced two-dimensional C_{60} polymers, Phys. Rev. B 59 (3) (1999) 1930–1936.
[22] L. Hou, X. Cui, B. Guan, et al., Synthesis of a monolayer fullerene network, Nature 606 (7914) (2022) 507–510.
[23] E. Meirzadeh, A.M. Evans, M. Rezaee, et al., A few-layer covalent network of fullerenes, Nature 613 (7942) (2023) 71–76.
[24] P. Simon, Y. Gogotsi, et al., Materials for electrochemical capacitors, Nat. Mater. 7 (11) (2008) 845–854.
[25] Y. Cao, V. Fatemi, S. Fang, et al., Unconventional superconductivity in magic-angle graphene superlattices, Nature 556 (7699) (2018) 43–50.
[26] Q. Burlingame, C. Coburn, X. Che, et al., Centimetre-scale electron diffusion in photoactive organic heterostructures, Nature 554 (7690) (2018) 77–80.
[27] F.A. Ma'Mari, T. Moorsom, G. Teobaldi, et al., Beating the Stoner criterion using molecular interfaces, Nature 524 (7563) (2015) 69–73.
[28] J. Zheng, L. Huang, C.-H. Cui, et al., Ambient-pressure synthesis of ethylene glycol catalyzed by C_{60}-buffered Cu/SiO_2, Science 376 (6590) (2022) 288–292.
[29] R. Zhang, Y. Li, X. Zhou, et al., Single-atomic platinum on fullerene C_{60} surfaces for accelerated alkaline hydrogen evolution, Nat. Commun. 14 (1) (2023) 2460.
[30] C. Zhang, W. Shen, K. Guo, et al., A pentagonal defect-rich metal-free carbon electrocatalyst for boosting acidic O_2 reduction to H_2O_2 production, J. Am. Chem. Soc. 145 (21) (2023) 11589–11598.
[31] K. Guo, Z. He, S. Lu, et al., A fullerene seeded strategy for facile construction of nitrogen-doped carbon nano-onions as robust electrocatalysts, Adv. Funct. Mater. 33 (29) (2023) 2302100.
[32] W. Kratschmer, L.D. Lamb, K. Fostiropoulos, et al., Solid C_{60}-a new form of carbon, Nature 347 (6291) (1990) 354–358.
[33] R.E. Haufler, J. Conceicao, L.P.F. Chibante, et al., Efficient production of C_{60} (buckminsterfullerene), $C_{60}H_{36}$, and the solvated buckide ion, J. Phys. Chem. 94 (24) (1990) 8634–8636.
[34] J.B. Howard, J.T. McKinnon, Y. Makarovsky, et al., Fullerenes C_{60} and C_{70} in flames, Nature 352 (6331) (1991) 139–141.
[35] K.O. Johansson, M.P. Head-Gordon, P.E. Schrader, et al., Resonance-stabilized hydrocarbon-radical chain reactions may explain soot inception and growth, Science 361 (6406) (2018) 997–1000.
[36] Z.Y. Gao, W.S. Jiang, D. Sun, et al., Synthesis of C_{3v}-$^{\#1911}C_{64}H_4$ using a low-pressure benzene/oxygen diffusion flame: Another pathway toward non-IPR fullerenes, Combust. Flame 157 (5) (2010) 966–969.
[37] Q.H. Weng, Q. He, T. Liu, et al., Simple combustion production and characterization of octahydro[60]fullerene with a non-IPR C_{60} cage, J. Am. Chem. Soc. 132 (43) (2010) 15093–15095.
[38] J.H. Chen, Z.Y. Gao, Q.H. Weng, et al., Combustion synthesis and electrochemical properties of the small hydrofullerene $C_{50}H_{10}$, Chem. Eur. J. 18 (11) (2012) 3408–3415.
[39] H.R. Tian, M.M. Chen, K. Wang, et al., An unconventional hydrofullerene $C_{66}H_4$ with symmetric heptagons retrieved in low-pressure combustion, J. Am. Chem. Soc. 141 (16) (2019) 6651–6657.
[40] M. Yamada, H. Kurihara, M. Suzuki, et al., $Sc_2@C_{66}$ revisited: An endohedral fullerene with scandium ions nestled within two unsaturated linear triquinanes, J. Am. Chem. Soc. 136 (21) (2014) 7611–7614.
[41] Y.Z. Tan, J. Li, F. Zhu, et al., Chlorofullerenes featuring triple sequentially fused pentagons, Nat. Chem. 2 (4) (2010) 269–273.
[42] C.L. Gao, X. Li, Y.Z. Tan, et al., Synthesis of long-sought C_{66} with exohedral stabilization, Angew. Chem. Int. Ed. 53 (30) (2014) 7853–7855.
[43] S. Yang, T. Wei, F. Jin, et al., When metal clusters meet carbon cages: Endohedral clusterfullerenes, Chem. Soc. Rev. 46 (16) (2017) 5005–5058.
[44] B. Elliott, L. Yu, L. Echegoyen, et al., A simple isomeric separation of D_{5h} and I_h $Sc_3N@C_{80}$ by selective chemical oxidation, J. Am. Chem. Soc. 127 (31) (2005) 10885–10888.
[45] Z. Ge, J.C. Duchamp, T. Cai, et al., Purification of endohedral trimetallic nitride fullerenes in a single, facile step, J. Am. Chem. Soc. 127 (46) (2005) 16292–16298.
[46] C.D. Angeli, T. Cai, J.C. Duchamp, et al., Purification of trimetallic nitride templated endohedral metallofullerenes by a chemical reaction of congeners with eutectic 9-methylanthracene, Chem. Mater. 20 (15) (2008) 4993–4997.
[47] S. Stevenson, K. Harich, H. Yu, et al., Nonchromatographic "stir and filter approach" (SAFA) for isolating $Sc_3N@C_{80}$ metallofullerenes, J. Am. Chem. Soc. 128 (27) (2006) 8829–8835.
[48] S. Stevenson, M.A. Mackey, C.E. Coumbe, et al., Rapid removal of D_{5h} isomer using the "stir and filter approach" and isolation of large quantities of isomerically pure $Sc_3N@C_{80}$ metallic nitride fullerenes, J. Am. Chem. Soc. 129 (19) (2007) 6072–6073.

[49] S. Stevenson, K.A. Rottinger, M. Fahim, et al., Tuning the selectivity of Gd_3N cluster endohedral metallofullerene reactions with Lewis acids, Inorg. Chem. 53 (24) (2014) 12939–12946.

[50] S. Stevenson, M.A. Mackey, J.E. Pickens, et al., Selective complexation and reactivity of metallic nitride and oxometallic fullerenes with Lewis acids and use as an effective purification method, Inorg. Chem. 48 (24) (2009) 11685–11690.

[51] K. Akiyama, T. Hamano, Y. Nakanishi, et al., Non-HPLC rapid separation of metallofullerenes and empty cages with $TiCl_4$ Lewis acid, J. Am. Chem. Soc. 134 (23) (2012) 9762–9767.

[52] S. Stevenson, H.R. Thompson, K.D. Arvola, et al., Isolation of $CeLu_2N@I_h$-C_{80} through a non-chromatographic, two-step chemical process and crystallographic characterization of the pyramidalized $CeLu_2N$ within the icosahedral cage, Chem. Eur. J. 21 (29) (2015) 10362–10368.

[53] F. Liu, L. Spree, D.S. Krylov, et al., Single-electron lanthanide-lanthanide bonds inside fullerenes toward robust redox-active molecular magnets, Acc. Chem. Res. 52 (10) (2019) 2981–2993.

[54] G. Gil-Ramírez, S.D. Karlen, A. Shundo, et al., A cyclic porphyrin trimer as a receptor for fullerenes, Org. Lett. 12 (15) (2010) 3544–3547.

[55] C. Fuertes-Espinosa, C. García-Simón, E. Castro, et al., A copper-based supramolecular nanocapsule that enables straightforward purification of Sc_3N-based endohedral metallofullerene soots, Chem. Eur. J. 23 (15) (2017) 3553–3557.

[56] C. Fuertes-Espinosa, A. Gómez-Torres, R. Morales-Martínez, et al., Purification of uranium-based endohedral metallofullerenes (EMFs) by selective supramolecular encapsulation and release, Angew. Chem. Int. Ed. 57 (35) (2018) 11294–11299.

[57] C. Fuertes-Espinosa, J. Murillo, M.E. Soto, et al., Highly selective encapsulation and purification of U-based C_{78}-EMFs within a supramolecular nanocapsule, Nanoscale 11 (47) (2019) 23035–23041.

[58] S. Stevenson, G. Rice, T. Glass, et al., Small-bandgap endohedral metallofullerenes in high yield and purity, Nature 401 (6748) (1999) 55–57.

[59] W. Shen, S. Hu, X. Lu, et al., Endohedral metallofullerenes: New structures and unseen phenomena, Chem. Eur. J. 26 (26) (2020) 5748–5757.

[60] L. Bao, P. Peng, X. Lu, et al., Bonding inside and outside fullerene cages, Acc. Chem. Res. 51 (3) (2018) 810–815.

[61] W. Shen, L. Bao, X. Lu, et al., Endohedral metallofullerenes: An ideal platform of sub-nano chemistry, Chin. J. Chem. 40 (2) (2022) 275–284.

[62] L. Bao, C. Pan, Z. Slanina, et al., Isolation and crystallographic characterization of the labile isomer of $Y@C_{82}$ cocrystallized with Ni(OEP): Unprecedented dimerization of pristine metallofullerenes, Angew. Chem. Int. Ed. 55 (32) (2016) 9234–9238.

[63] S. Hu, T. Liu, W. Shen, et al., Isolation and structural characterization of $Er@C_{2v}(9)$-C_{82} and $Er@C_s(6)$-C_{82}: Regioselective dimerization of a pristine endohedral metallofullerene induced by cage symmetry, Inorg. Chem. 58 (3) (2019) 2177–2182.

[64] M. Suzuki, M. Yamada, Y. Maeda, et al., The unanticipated dimerization of $Ce@C_{2v}(9)$-C_{82} upon co-crystallization with Ni(octaethylporphyrin) and comparison with monomeric $M@C_{2v}(9)$-C_{82} (M = La, Sc, and Y), Chem. Eur. J. 22 (50) (2016) 18115–18122.

[65] L. Feng, T. Tsuchiya, T. Wakahara, et al., Synthesis and characterization of a bisadduct of $La@C_{82}$, J. Am. Chem. Soc. 128 (18) (2006) 5990–5991.

[66] M. Yamada, H. Kurihara, M. Suzuki, et al., Hiding and recovering electrons in a dimetallic endohedral fullerene: Air-stable products from radical additions, J. Am. Chem. Soc. 137 (1) (2015) 232–238.

[67] L. Bao, M. Chen, C. Pan, et al., Crystallographic evidence for direct metal–metal bonding in a stable open-shell $La_2@I_h$-C_{80} derivative, Angew. Chem. Int. Ed. 55 (13) (2016) 4242–4246.

[68] Z. Wang, R. Kitaura, H. Shinohara, et al., Metal-dependent stability of pristine and functionalized unconventional dimetallofullerene $M_2@I_h$-C_{80}, J. Phys. Chem. C 118 (25) (2014) 13953–13958.

[69] F. Liu, D.S. Krylov, L. Spree, et al., Single molecule magnet with an unpaired electron trapped between two lanthanide ions inside a fullerene, Nat. Commun. 8 (2017) 16098–16107.

[70] W. Shen, L. Bao, Y. Wu, et al., $Lu_2@C_{2n}$ (2n = 82, 84, 86): Crystallographic evidence of direct Lu–Lu bonding between two divalent lutetium ions inside fullerene cages, J. Am. Chem. Soc. 139 (29) (2017) 9979–9984.

[71] W. Shen, L. Bao, S. Hu, et al., Crystallographic characterization of Lu_2C_{2n} (2n = 76–90): Cluster selection by cage size, Chem. Sci. 10 (3) (2019) 829–836.

[72] C. Pan, W. Shen, L. Yang, et al., Crystallographic characterization of Y_2C_{2n} (2n = 82, 88–94): Direct Y–Y bonding and cage-dependent cluster evolution, Chem. Sci. 10 (17) (2019) 4707–4713.

[73] S. Hu, W. Shen, L. Yang, et al., Crystallographic and theoretical investigations of $Er_2@C_{2n}$ (2n=82, 84, 86): Indication of distance-dependent metal–metal bonding nature, Chem. Eur. J. 25 (49) (2019) 11538–11544.

[74] S. Stevenson, A.J. Rothgeb, K.R. Tepper, et al., Isolation and crystallographic characterization of two, nonisolated pentagon endohedral fullerenes: $Ho_3N@C_2(22010)$-C_{78} and $Tb_3N@C_2(22010)$-C_{78}, Chem. Eur. J. 25 (54) (2019) 12545–12551.

[75] L. Feng, M. Zhang, Y. Hao, et al., Endohedrally stabilized C_{70} isomer with fused pentagons characterized by crystallography, Dalton Trans. 45 (19) (2016) 8142–8148.

[76] A. Liu, M. Nie, Y. Hao, et al., $Ho_2O@C_{74}$: Ho_2O cluster expands within a small non-IPR fullerene cage of $C_2(13333)$-C_{74}, Inorg. Chem. 58 (8) (2019) 4774–4781.

[77] T. Guo, M.D. Diener, Y. Chai, et al., Uranium stabilization of C_{28} - a tetravalent fullerene, Science 257 (5077) (1992) 1661–1664.

[78] B.I. Dunlap, O.D. Haeberlen, N. Roesch, et al., Asymmetric localization of titanium in carbon molecule C_{28}, J. Phys. Chem. 96 (23) (1992) 9095–9097.

[79] B.P. Cao, M. Hasegawa, K. Okada, et al., EELS and C^{13} NMR characterization of pure $Ti_2@C_{80}$ metallofullerene, J. Am. Chem. Soc. 123 (39) (2001) 9679–9680.

[80] B.P. Cao, K. Suenaga, T. Okazaki, et al., Production, isolation, and EELS characterization of $Ti_2@C_{84}$ dititanium metallofullerenes, J. Phys. Chem. B 106 (36) (2002) 9295–9298.

[81] T. Yumura, Y. Sato, K. Suenaga, et al., Which do endohedral Ti_2C_{80} metallofullerenes prefer energetically: $Ti@C_{80}$ or $Ti_2C_2@C_{78}$? A theoretical study, J. Phys. Chem. B 109 (43) (2005) 20251–20255.

[82] Y. Zhao, M. Li, R. Zhao, et al., Unmasking the optimal isomers of Ti_2C_{84}: $Ti_2C_2@C_{82}$ instead of $Ti_2@C_{84}$, J. Phys. Chem. C 122 (24) (2018) 13148–13155.

[83] F.F. Li, N. Chen, M. Mulet-Gas, et al., $Ti_2S@D_{3h}(24109)$-C_{78}: A sulfide cluster metallofullerene containing only transition metals inside the cage, Chem. Sci. 4 (9) (2013) 3404–3410.

[84] P. Yu, W. Shen, L. Bao, et al., Trapping an unprecedented Ti_3C_3 unit inside the icosahedral C_{80} fullerene: A crystallographic survey, Chem. Sci. 10 (47) (2019) 10925–10930.

[85] P. Yu, L. Bao, L. Yang, et al., Crystallographic characterization of $Ti_2C_2@D_{3h}(5)$-C_{78}, $Ti_2C_2@C_{3v}(8)$-C_{82}, and $Ti_2C_2@C_s(6)$-C_{82}: Identification of unsupported Ti_2C_2 cluster with cage-dependent configurations, Inorg. Chem. 59 (13) (2020) 9416–9423.

[86] S. Yang, C. Chen, A.A. Popov, et al., An endohedral titanium(III) in a cluster-fullerene: Putting a non-group-III metal nitride into the C_{80}-I_h fullerene cage, Chem. Commun. (42) (2009) 6391–6393.

[87] C.B. Chen, F.P. Liu, S.J. Li, et al., Titanium/yttrium mixed metal nitride cluster-fullerene $TiY_2N@C_{80}$: Synthesis, isolation and effect of the group-III metal, Inorg. Chem. 51 (2012) 3039–3045.

[88] K. Junghans, C. Schlesier, A. Kostanyan, et al., Methane as a selectivity booster in the arc-discharge synthesis of endohedral fullerenes: Selective synthesis of the single-molecule magnet $Dy_2TiC@C_{80}$ and its congener $Dy_2TiC_2@C_{80}$, Angew. Chem. Int. Ed. 54 (45) (2015) 13411–13415.

[89] A.L. Svitova, K.B. Ghiassi, C. Schlesier, et al., Endohedral fullerene with μ_3-carbido ligand and titanium-carbon double bond stabilized inside a carbon cage, Nat. Commun. 5 (1) (2014) 3568–3576.

[90] K. Junghans, K.B. Ghiassi, N.A. Samoylova, et al., Synthesis and isolation of the titanium–scandium endohedral fullerenes—$Sc_2TiC@I_h$-C_{80}, $Sc_2TiC@D_{5h}$-C_{80} and $Sc_2TiC_2@I_h$-C_{80}: Metal size tuning of the Ti^{IV}/Ti^{III} redox potentials, Chem. Eur. J. 22 (37) (2016) 13098–13107.

[91] T. Wei, S. Wang, X. Lu, et al., Entrapping a group-VB transition metal, vanadium, within an endohedral metallofullerene: $V_xSc_{3-x}N@I_h$-C_{80} (x = 1, 2), J. Am. Chem. Soc. 138 (1) (2016) 207–214.

[92] T. Wei, F. Jin, R. Guan, et al., Blending non-group-3 transition metal and rare-earth metal into a C_{80} fullerene cage with D_{5h} symmetry, Angew. Chem. Int. Ed. 57 (32) (2018) 10273–10277.

[93] R. Guan, Z.C. Chen, J. Huang, et al., Self-driven carbon atom implantation into fullerene embedding metal–carbon cluster, PNAS 119 (39) (2022) e2202563119.

[94] W. Cai, R. Morales-Martinez, X. Zhang, et al., Single crystal structures and theoretical calculations of uranium endohedral metallofullerenes ($U@C_{2n}$, 2n = 74, 82) show cage isomer dependent oxidation states for U, Chem. Sci. 8 (8) (2017) 5282–5290.

[95] W. Cai, L. Abella, J. Zhuang, et al., Synthesis and characterization of non-isolated-pentagon-rule actinide endohedral metallofullerenes $U@C_1(17418)$-C_{76}, $U@C_1(28324)$-C_{80}, and $Th@C_1(28324)$-C_{80}: Low-symmetry cage selection directed by a yetravalent Ion, J. Am. Chem. Soc. 140 (51) (2018) 18039–18050.

[96] X. Zhang, W. Li, L. Feng, et al., A diuranium carbide cluster stabilized inside a C_{80} fullerene cage, Nat. Commun. 9 (1) (2018) 2753.

[97] X. Li, Y.R. Yao, W. Yang, et al., Crystallographic and spectroscopic characterization of a mixed actinide–lanthanide carbide cluster stabilized inside an $I_h(7)$-C_{80} fullerene cage, Chem. Commun. 56 (27) (2020) 3867–3870.

[98] J. Zhuang, L. Abella, D.-C. Sergentu, et al., Diuranium(IV) carbide cluster U_2C_2 stabilized inside fullerene cages, J. Am. Chem. Soc. 141 (51) (2019) 20249–20260.

[99] Q. Meng, L. Abella, W. Yang, et al., $UCN@C_s(6)$-C_{82}: An encapsulated triangular UCN cluster with ambiguous U oxidation state [U(III) versus U(I)], J. Am. Chem. Soc. 143 (39) (2021) 16226–16234.

[100] Q. Meng, L. Abella, Y.-R. Yao, et al., A charged diatomic triple-bonded U≡N species trapped in C82 fullerene cages, Nat. Commun. 13 (2022) 7192.

[101] H. Jiang, X. Yu, M. Guo, et al., USc_2C_2 and USc_2NC clusters with U–C triple bond character stabilized inside fullerene cages, J. Am. Chem. Soc. 145 (10) (2023) 5645–5654.

[102] P.W. Dunk, N.K. Kaiser, C.L. Hendrickson, et al., Closed network growth of fullerenes, Nat. Commun. 3 (2012) 855–864.

[103] B. Saha, S. Irle, K. Morokuma, et al., Hot giant fullerenes eject and capture C_2 molecules: QM/MD simulations with constant density, J. Phys. Chem. C 115 (46) (2011) 22707–22716.

[104] L. Bao, P. Yu, C. Pan, et al., Crystallographic identification of $Eu@C_{2n}$ (2n = 88, 86 and 84): Completing a transformation map for existing metallofullerenes, Chem. Sci. 10 (10) (2019) 2153–2158.

[105] L. Bao, Y. Li, P. Yu, et al., Preferential formation of mono-metallofullerenes governed by the encapsulation energy of the metal elements: A case study on $Eu@C_{2n}$ (2n=74–84) revealing a general rule, Angew. Chem. Int. Ed. 59 (13) (2020) 5259–5262.

[106] C.H. Chen, L. Abella, M.R. Cerón, et al., Zigzag Sc_2C_2 carbide cluster inside a [88]fullerene cage with one heptagon, $Sc_2C_2@C_s$(hept)-C_{88}: A kinetically trapped fullerene formed by C_2 insertion? J. Am. Chem. Soc. 138 (39) (2016) 13030–13037.

[107] C.H. Chen, K.B. Ghiassi, M.R. Cerón, et al., Beyond the butterfly: $Sc_2C_2@C_{2v}(9)$-C_{86}, an endohedral fullerene containing a planar, twisted Sc_2C_2 unit with remarkable crystalline order in an unprecedented carbon cage, J. Am. Chem. Soc. 137 (32) (2015) 10116–10119.

[108] W. Cai, J. Alvarado, A. Metta-Magaña, et al., Interconversions between uranium mono-metallofullerenes: Mechanistic implications and role of asymmetric cages, J. Am. Chem. Soc. 142 (30) (2020) 13112–13119.
[109] W. Cai, F.F. Li, L. Bao, et al., Isolation and crystallographic characterization of $La_2C_2@C_s$(574)-C_{102} and $La_2C_2@C_2$(816)-C_{104}: Evidence for the top-down formation mechanism of fullerenes, J. Am. Chem. Soc. 138 (20) (2016) 6670–6675.
[110] J. Zhang, F.L. Bowles, D.W. Bearden, et al., A missing link in the transformation from asymmetric to symmetric metallofullerene cages implies a top-down fullerene formation mechanism, Nat. Chem. 5 (10) (2013) 880–885.
[111] A. Chuvilin, U. Kaiser, E. Bichoutskaia, et al., Direct transformation of graphene to fullerene, Nat. Chem. 2 (6) (2010) 450–453.
[112] C. Chen, G. Xing, J. Wang, et al., Multihydroxylated $[Gd@C_{82}(OH)_{22}]_n$ nanoparticles: antineoplastic activity of high efficiency and low toxicity, Nano Lett. 5 (10) (2005) 2050–2057.
[113] S.g. Kang, G. Zhou, P. Yang, et al., Molecular mechanism of pancreatic tumor metastasis inhibition by $Gd@C_{82}(OH)_{22}$ and its implication for de novo design of nanomedicine, PNAS 109 (38) (2012) 15431–15436.
[114] H. Meng, G. Xing, E. Blanco, et al., Gadolinium metallofullerenol nanoparticles inhibit cancer metastasis through matrix metalloproteinase inhibition: Imprisoning instead of poisoning cancer cells, Nanomed.-Nanotechnol. 8 (2) (2012) 136–146.
[115] Y. Zhou, R. Deng, M. Zhen, et al., Amino acid functionalized gadofullerene nanoparticles with superior antitumor activity via destruction of tumor vasculature in vivo, Biomaterials 133 (2017) 107–118.
[116] M. Zhen, C. Shu, J. Li, et al., A highly efficient and tumor vascular-targeting therapeutic technique with size-expansible gadofullerene nanocrystals, Sci. China Mater. 58 (10) (2015) 799–810.
[117] X. Li, M. Zhen, R. Deng, et al., RF-assisted gadofullerene nanoparticles induces rapid tumor vascular disruption by down-expression of tumor vascular endothelial cadherin, Biomaterials 163 (2018) 142–153.
[118] Y. Zhang, C. Shu, M. Zhen, et al., A novel bone marrow targeted gadofullerene agent protect against oxidative injury in chemotherapy, Sci. China Mater. 60 (9) (2017) 866–880.
[119] J. Li, M. Guan, T. Wang, et al., $Gd@C_{82}$-(ethylenediamine)$_8$ nanoparticle: A new high-efficiency water-soluble ROS scavenger, ACS Appl. Mater. Interfaces 8 (39) (2016) 25770–25776.
[120] T. Wang, C. Wang, et al., Functional metallofullerene materials and their applications in nanomedicine, magnetics, and electronics, Small 15 (48) (2019) 1901522.
[121] R. Westerström, J. Dreiser, C. Piamonteze, et al., An endohedral single-molecule magnet with long relaxation times: $DySc_2N@C_{80}$, J. Am. Chem. Soc. 134 (24) (2012) 9840–9843.
[122] D.S. Krylov, F. Liu, S.M. Avdoshenko, et al., Record-high thermal barrier of the relaxation of magnetization in the nitride clusterfullerene $Dy_2ScN@C_{80}$-I_h, Chem. Commun. 53 (56) (2017) 7901–7904.
[123] Y. Hao, G. Velkos, S. Schiemenz, et al., Using internal strain and mass to modulate Dy•••Dy coupling and relaxation of magnetization in heterobimetallic metallofullerenes $DyM_2N@C_{80}$ and $Dy_2MN@C_{80}$ (M = Sc, Y, La, Lu), Inorg. Chem. Front. 10 (2) (2023) 468–484.
[124] W. Yang, G. Velkos, F. Liu, et al., Single molecule magnets: Single molecule magnetism with strong magnetic anisotropy and enhanced Dy•••Dy coupling in three isomers of Dy-oxide clusterfullerene $Dy_2O@C_{82}$, Adv. Sci. 6 (20) (2019) 1970119.
[125] G. Velkos, W. Yang, Y.-R. Yao, et al., Shape-adaptive single-molecule magnetism and hysteresis up to 14K in oxide clusterfullerenes $Dy_2O@C_{72}$ and $Dy_2O@C_{74}$ with fused pentagon pairs and flexible Dy–(μ_2-O)–Dy angle, Chem. Sci. 11 (18) (2020) 4766–4772.
[126] C.H. Chen, D.S. Krylov, Stanislav M. Avdoshenko, et al., Selective arc-discharge synthesis of Dy_2S-clusterfullerenes and their isomer-dependent single molecule magnetism, Chem. Sci. 8 (9) (2017) 6451–6465.
[127] C. Schlesier, L. Spree, A. Kostanyan, et al., Strong carbon cage influence on the single molecule magnetism in Dy–Sc nitride clusterfullerenes, Chem. Commun. 54 (70) (2018) 9730–9733.
[128] F. Liu, G. Velkos, D.S. Krylov, et al., Air-stable redox-active nanomagnets with lanthanide spins radical-bridged by a metal–metal bond, Nat. Commun. 10 (1) (2019) 571–582.
[129] G. Velkos, D.S. Krylov, K. Kirkpatrick, et al., High blocking temperature of magnetization and giant coercivity in the azafullerene $Tb_2@C_{79}N$ with a single-electron terbium–terbium bond, Angew. Chem. Int. Ed. 58 (18) (2019) 5891–5896.
[130] D. Ielmini, H.S.P. Wong, et al., In-memory computing with resistive switching devices, Nat. Electron. 1 (6) (2018) 333–343.
[131] W. Zhang, R. Mazzarello, M. Wuttig, et al., Designing crystallization in phase-change materials for universal memory and neuro-inspired computing, Nat. Rev. Mater. 4 (3)) (2019) 150–168.
[132] J. Grollier, D. Querlioz, K.Y. Camsari, et al., Neuromorphic spintronics, Nat. Electron. 3 (7) (2020) 360–370.
[133] R. Guo, W. Lin, X. Yan, et al., Ferroic tunnel junctions and their application in neuromorphic networks, Appl. Phys. Rev. 7 (1) (2020) 011304.
[134] K. Zhang, C. Wang, M. Zhang, et al., A $Gd@C_{82}$ single-molecule electret, Nat. Nanotech. 15 (12) (2020) 1019–1024.
[135] A. Jaroš, E.F. Bonab, M. Straka, et al., Fullerene-based switching molecular diodes controlled by oriented external electric fields, J. Am. Chem. Soc. 141 (50) (2019) 19644–19654.
[136] J. Li, S. Hou, Y.-R. Yao, et al., Room-temperature logic-in-memory operations in single-metallofullerene devices, Nat. Mater. 21 (8) (2022) 917–923.
[137] P. Li, Z. Jiang, X. Huang, et al., Nitrofullerene as an electrolyte-compatible additive for high-performance sodium metal batteries, Nano Energy 89 (2021) 106396.
[138] J. Xiang, W. Shen, Z. Guo, et al., A supramolecular complex of C_{60}–S with high–density active sites as a cathode for lithium–sulfur batteries, Angew. Chem. Int. Ed. 60 (26) (2021) 14313–14318.

Author profile

Wenting Cai is currently an associate professor at Xi'an Jiaotong University. She is the recipient of The Young Talent Support Plan of Xi'an Jiaotong University (2021). Her research interests include the generation and characterization of synthetic carbon allotropes, along with exploring their potential applications in single-molecule magnets and electrocatalysis. Her research work has been published in the high-impact journals including *Nature Energy, J. Am. Chem. Soc.*

Luis Echegoyen served as the Robert A. Welch Professor of Chemistry at the University of Texas at El Paso from August 2010 until his retirement in 2021 and was President of the American Chemical Society in 2020. Luis was also the Director of the Chemistry Division of the National Science Foundation from August 2006 until August 2010 and served as Chair for the Department of Chemistry at Clemson University from 2002 until 2006. Luis has published > 515 articles, including 49 book chapters.

Xing Lu (BRID: 09855.00.12903) is a full professor in Huazhong University of Science and Technology. He is the recipient of The Ambassador Award from Chinese Embassy in Japan (2009), The Osawa Award from Fullerenes and Nanotubes Research Society of Japan (2011) and The National Science Fund for Distinguished Young Scholars (2019). His research interests lie in the rational design and facile generation of novel hybrid carbon materials with applications in energy storage and conversion. He has published more than 200 peer-reviewed papers in international journals with > 50 at *J. Am. Chem. Soc.* and *Angew. Chem. Int. Ed.*